Commun. Comput. Phys.
doi: 10.4208/cicp.300815.180416a

Vol. **21**, No. 1, pp. 93-125
January 2017

A Compact Scheme for Coupled Stochastic Nonlinear Schrödinger Equations

Chuchu Chen[1], Jialin Hong[1], Lihai Ji[2,*] and Linghua Kong[3]

[1] *Institute of Computational Mathematics and Scientific/Engineering Computing, Academy of Mathematics and Systems Science, Chinese Academy of Sciences, Beijing 100190, China.*
[2] *Institute of Applied Physics and Computational Mathematics, Beijing 100094, China.*
[3] *School of Mathematics and Information Science, Jiangxi Normal University, Nanchang, Jiangxi 330022, China.*

Received 30 August 2015; Accepted (in revised version) 18 April 2016

Abstract. In this paper, we propose a compact scheme to numerically study the coupled stochastic nonlinear Schrödinger equations. We prove that the compact scheme preserves the discrete stochastic multi-symplectic conservation law, discrete charge conservation law and discrete energy evolution law almost surely. Numerical experiments confirm well the theoretical analysis results. Furthermore, we present a detailed numerical investigation of the optical phenomena based on the compact scheme. By numerical experiments for various amplitudes of noise, we find that the noise accelerates the oscillation of the soliton and leads to the decay of the solution amplitudes with respect to time. In particular, if the noise is relatively strong, the soliton will be totally destroyed. Meanwhile, we observe that the phase shift is sensibly modified by the noise. Moreover, the numerical results present inelastic interaction which is different from the deterministic case.

AMS subject classifications: 60H15, 60H35, 37K05

Key words: Coupled stochastic nonlinear Schrödinger equations, compact scheme, stochastic multi-symplectic conservation law, energy evolution law, charge conservation law, soliton evolution, soliton interaction.

1 Introduction

The propagation of optical solitons in a nonlinear dispersive optical fiber is governed by the well-known coupled nonlinear Schrödinger (CNLS) equations of the form [5]

*Corresponding author. *Email addresses:* chenchuchu@lsec.cc.ac.cn (C. Chen), hjl@lsec.cc.ac.cn (J. Hong), jilihai@lsec.cc.ac.cn (L. Ji), konglh@mail.ustc.edu.cn (L. Kong)

 ©2016 Global-Science Press

https://doi.org/10.4208/cicp.300815.180416a Published online by Cambridge University Press

$$\begin{aligned} \mathrm{i}u_t+\alpha u_{xx}+\left(\sigma|u|^2+\beta|v|^2\right)u=0,\\ \mathrm{i}v_t+\alpha v_{xx}+\left(\sigma|v|^2+\beta|u|^2\right)v=0, \end{aligned} \tag{1.1}$$

where u, v are complex amplitudes or envelops of two wave packets, α, σ and β are the group velocity dispersion, selfphase modulation parameter and cross-modulation coefficient, respectively; x and t represent the spatial and temporal coordinates. Due to their intrinsic stability, optical solitons have been proposed to use as information carrier for the long-distance fiber optic communications and the optical signal processing. A major limitation for the soliton applications is the multi-soliton evolution and interaction. To understand the nature and consequence of soliton evolution and interaction, extensive theoretical and experimental investigations have been carried out [4, 8, 10, 12–14].

In practical circumstances, stochasticity is common in optical soliton communications. Generally speaking, the stochasticity can be classified into two basic types: the homogenous and nonhomogeneous [3]. For the homogenous case, stochasticity is presented in the input pulse with random initial values; for the nonhomogeneous case, due to the factor such as the random perturbation of the dispersion term, which may be originated by random variation of the optical fiber parameters, etc. Indeed, [17] studies the stability of solitons in a fiber with randomly oriented birefringence, and observes that the soliton does not split even at high values of the average birefringence. Meanwhile, in [16], a nonlinear optical fiber with random birefringence is modeled by a system of NLS equations with stochastic coupling, and the effects of randomly varying birefringence on the dynamics of propagating optical pulses are analyzed. Recently, [15] investigates the dynamics of the bound vector solitons for the coupled nonlinear Schrödinger equations with the random optical fiber parameters, and finds that soliton switching is closely influenced by the amplitudes of stochastic perturbations. This paper is devoted to the study of the influence of a noise term as the potential of CNLS equations on the propagation and interaction of solitons. It may cause drastically changes of the qualitative behavior of the solitons. The stochastic system of our interest is

$$\begin{aligned} \mathrm{i}\mathrm{d}u+\alpha u_{xx}\mathrm{d}t+\left(\sigma|u|^2+\beta|v|^2\right)u\mathrm{d}t=\varepsilon u\circ\mathrm{d}W(t),\\ \mathrm{i}\mathrm{d}v+\alpha v_{xx}\mathrm{d}t+\left(\sigma|v|^2+\beta|u|^2\right)v\mathrm{d}t=\varepsilon v\circ\mathrm{d}W(t), \end{aligned} \tag{1.2}$$

where ε is a nonnegative and real-valued constant which denotes the amplitude of the noise. The $\circ$ in the right-hand side of (1.2) means that the product is of Stratonovich type, and W denotes a real-valued space-time noise.

In this work, we use numerical simulations to study qualitatively the solutions of (1.2). This leads to choose a method which allows high resolution, compactness and economy. Furthermore, numerical methods preserving the structure characteristics of equations should be much better in preservation of physical properties and long time

https://doi.org/10.4208/cicp.300815.180416a Published online by Cambridge University Press

simulation of coupled stochastic nonlinear Schrödinger (CSNLS) equations [6]. Thus, we propose a compact scheme which, in the deterministic case, has shown to be suitable for computing complicated coupled problem; for more details see [9, 11]. By theoretical and numerical analysis, we show that the scheme can preserve the discrete stochastic multi-symplectic conservation law, discrete charge conservation law and discrete energy evolution law almost surely for arbitrary number of CSNLS equations. Numerical simulations match the theoretical analysis results well and verify the efficiency of the scheme.

Besides, we also present a detailed numerical investigation of some optical phenomena in the framework of CSNLS equations based on the compact scheme. By choosing different initial data and various amplitudes of noise, it is observed that the noise introduces the oscillation to the profiles and could create new waves. The interaction of the soliton and waves generated by the noise leads to the decrease of the solution amplitudes, and exhibits inelastic characteristic which is different from the deterministic case. Besides, the noise changes the position of the peak. In particular, the phenomena of phase shift are more significant in the long propagation interval or with large noise amplitude. Furthermore, we also consider the cases of three CSNLS (3-CSNLS) equations and four CSNLS (4-CSNLS) equations and find that they are more sensitive to the perturbation of noise than that of two coupled case.

The rest of this paper is organized as follows. In Section 2, we present some geometric and physical properties about CSNLS equations. It is shown that the phase flow of equations preserves the stochastic multi-symplectic structure in phase space, and possesses charge conservation law and energy evolution law. In Section 3, we propose a compact scheme and show that the scheme preserves the discrete stochastic multi-symplectic conservation law, discrete charge conservation law and discrete energy evolution law almost surely. In Section 4, numerical experiments with different initial values, coefficients and scales of noise are performed to discuss the effects of random potential on the evolution of a single soliton, the interaction of multi-solitons and the splitting of a profile into more solitons. Finally, concluding remarks are presented in Section 5.

2 Preliminary results

2.1 Stochastic framework

Let $(\Omega,\mathcal{F},P)$ be the probability space with filtration $\{\mathcal{F}_t\}_{0\le t\le T}$ and let $\{\beta_k\}_{k\in\mathbb{N}}$ be a sequence of independent Brownian motions associated to this filtration. Given $\{e_k\}_{k\in\mathbb{N}}$ an orthonormal basis of $L^2(\mathbb{R};\mathbb{R})$ (the space of real-valued square integrable functions on $\mathbb{R}$), and a linear operator ϕ on $L^2(\mathbb{R};\mathbb{R})$, then process

$$W(t,x,\omega)=\sum_{k=0}^{\infty}\beta_k(t,\omega)\phi e_k(x),\quad 0\le t\le T,\quad x\in\mathbb{R},\quad \omega\in\Omega \tag{2.1}$$

is a Wiener process on $L^2(\mathbb{R};\mathbb{R})$, with covariance operator $\phi\phi^*$. Furthermore, we assume that $\phi\in \mathrm{HS}(L^2(\mathbb{R};\mathbb{R}),H^1(\mathbb{R};\mathbb{R}))$ throughout this paper, where $H^1(\mathbb{R};\mathbb{R})$ represents the

https://doi.org/10.4208/cicp.300815.180416a Published online by Cambridge University Press

Sobolev space and $\mathrm{HS}(U,V)$ denotes the space of all Hilbert-Schmidt operators from the separable Hilbert space U to another separable Hilbert space V with the norm given by

$$\|Q\|_{\mathrm{HS}(U,V)}=\Big(\sum_{m\in\mathbb{N}}\|Qf_m\|_V^2\Big)^{\frac{1}{2}},\qquad \forall\, Q\in\mathrm{HS}(U,V)$$

with $\{f_m\}_{m\in\mathbb{N}}$ being an orthonormal basis of U.

We will use the equivalent Itô equations of (1.2). Defining the function

$$F_\phi(x)=\sum_{k=0}^{\infty}(\phi e_k(x))^2,\quad x\in\mathbb{R}, \tag{2.2}$$

which is independent of the basis $\{e_k\}_{k\in\mathbb{N}}$, the equivalent Itô equations could be written as

$$\begin{aligned}
&\mathrm{i}\mathrm{d}u+\alpha u_{xx}\mathrm{d}t+\Big(\sigma|u|^2+\beta|v|^2\Big)u\mathrm{d}t+\mathrm{i}\frac{\varepsilon^2}{2}uF_\phi\mathrm{d}t=\varepsilon u\mathrm{d}W(t),\\
&\mathrm{i}\mathrm{d}v+\alpha v_{xx}\mathrm{d}t+\Big(\sigma|v|^2+\beta|u|^2\Big)v\mathrm{d}t+\mathrm{i}\frac{\varepsilon^2}{2}vF_\phi\mathrm{d}t=\varepsilon v\mathrm{d}W(t).
\end{aligned} \tag{2.3}$$

2.2 Stochastic multi-symplectic formulation of the CSNLS equations

One of the inherent canonical properties of Hamiltonian system is the symplecticity or multi-symplecticity of its flow. The analysis of multi-symplecticity of stochastic Hamiltonian partial differential equations is presented in [7] for instance. In this part, we will focus on the multi-symplectic property of CSNLS equations (1.2).

Assume that $u(x,t)=r_1(x,t)+\mathrm{i}s_1(x,t)$, $v(x,t)=r_2(x,t)+\mathrm{i}s_2(x,t)$, where r_1, s_1, r_2, s_2 are real-valued functions. By introducing additional auxiliary variables $p_1=\alpha\frac{\partial r_1}{\partial x}$, $q_1=\alpha\frac{\partial s_1}{\partial x}$, $p_2=\alpha\frac{\partial r_2}{\partial x}$, $q_2=\alpha\frac{\partial s_2}{\partial x}$ and defining $z=(r_1,s_1,r_2,s_2,p_1,q_1,p_2,q_2)^T$, Eqs. (1.2) can be rewritten as a system of stochastic Hamiltonian partial differential equations

$$K\mathrm{d}z_t+Lz_x\mathrm{d}t=\nabla_z S_1(z)\mathrm{d}t+\nabla_z S_2(z)\circ\mathrm{d}W,\quad z\in\mathbb{R}^8, \tag{2.4}$$

where

$$\begin{aligned}
&S_1(z)=\frac{\sigma}{4}\Big[(r_1^2+s_1^2)^2+(r_2^2+s_2^2)^2\Big]+\frac{\beta}{2}(r_1^2+s_1^2)(r_2^2+s_2^2)+\frac{1}{2\alpha}\Big(p_1^2+q_1^2+p_2^2+q_2^2\Big),\\
&S_2(z)=-\frac{\varepsilon}{2}\Big(r_1^2+s_1^2+r_2^2+s_2^2\Big),
\end{aligned}$$

and

$$K=\begin{pmatrix}J&\mathbf{0}&\mathbf{0}&\mathbf{0}\\ \mathbf{0}&J&\mathbf{0}&\mathbf{0}\\ \mathbf{0}&\mathbf{0}&\mathbf{0}&\mathbf{0}\\ \mathbf{0}&\mathbf{0}&\mathbf{0}&\mathbf{0}\end{pmatrix}_{8\times8},\quad L=\begin{pmatrix}\mathbf{0}&\mathbf{0}&-I&\mathbf{0}\\ \mathbf{0}&\mathbf{0}&\mathbf{0}&-I\\ I&\mathbf{0}&\mathbf{0}&\mathbf{0}\\ \mathbf{0}&I&\mathbf{0}&\mathbf{0}\end{pmatrix}_{8\times8},$$

https://doi.org/10.4208/cicp.300815.180416a Published online by Cambridge University Press

where I is 2×2 identity matrix and

$$J=\begin{pmatrix} 0 & 1 \\ -1 & 0 \end{pmatrix},$$

with 0 means the number zero and **0** means matrix zero.

Similarly to the proof of Theorem 2.2 in [7], we can obtain the following result.

Theorem 2.1. *The system* (2.4) *possesses the stochastic multi-symplectic conservation law locally*

$$\mathrm{d}_t\omega(x,t)+\partial_x\kappa(x,t)=0, \tag{2.5}$$

i.e.,

$$\int_{x_0}^{x_1}\omega(x,t_1)\mathrm{d}x+\int_{t_0}^{t_1}\kappa(x_1,t)\mathrm{d}t=\int_{x_0}^{x_1}\omega(x,t_0)\mathrm{d}x+\int_{t_0}^{t_1}\kappa(x_0,t)\mathrm{d}t,$$

where $\omega=\frac{1}{2}\mathrm{d}z\wedge K\mathrm{d}z$, $\kappa=\frac{1}{2}\mathrm{d}z\wedge L\mathrm{d}z$ *are the differential 2-forms associated with the two skew-symmetric matrices K and L, respectively, the notation* $\wedge$ *means the wedge product, and* $(x_0,x_1)\times(t_0,t_1)$ *is the local definition domain of* $z(x,t)$.

2.3 Conservation laws

As is well known, the deterministic CNLS equations (1.1) have some invariants. These invariants are important criteria in measuring whether a numerical method is good or not. Similarly, we can also obtain several conservative properties for CSNLS equations (1.2). These are stated in the following theorems.

Theorem 2.2. *The CSNLS equations* (1.2) *possess the charge conservation laws almost surely*

$$\int_{\mathbb{R}}|u(x,t)|^2\mathrm{d}x=\int_{\mathbb{R}}|u(x,0)|^2\mathrm{d}x,\quad \int_{\mathbb{R}}|v(x,t)|^2\mathrm{d}x=\int_{\mathbb{R}}|v(x,0)|^2\mathrm{d}x. \tag{2.6}$$

Proof. The proof is based on the application of Itô formula to functional $Q(u)=\int_{\mathbb{R}}|u|^2\mathrm{d}x$. Since $Q(u)$ is Fréchet derivable, the derivatives of $Q(u)$ along direction ψ and (ψ,ϕ) are as follows:

$$DQ(u)(\psi)=2\mathfrak{Re}\int_{\mathbb{R}}u\bar{\psi}\mathrm{d}x,\qquad D^2Q(u)(\psi,\phi)=2\mathfrak{Re}\int_{\mathbb{R}}\psi\bar{\phi}\mathrm{d}x.$$

From Itô formula, we have

$$\begin{aligned}\int_{\mathbb{R}}|u(t)|^2\mathrm{d}x&=\int_{\mathbb{R}}|u(0)|^2\mathrm{d}x+\int_0^t DQ(u(s))(\mathrm{d}u)+\frac{1}{2}\int_0^t\mathrm{Tr}\Big[D^2Q(u)\big(-\mathrm{i}\varepsilon u\phi\big)\big(-\mathrm{i}\varepsilon u\phi\big)^*\Big]\mathrm{d}s\\&=\int_{\mathbb{R}}|u(0)|^2\mathrm{d}x+2\int_0^t\mathfrak{Re}\int_{\mathbb{R}}u\Big(-\mathrm{i}\alpha\bar{u}_{xx}-\mathrm{i}(\sigma|u|^2+\beta|v|^2)\bar{u}-\frac{\varepsilon^2}{2}\bar{u}F_\phi\Big)\mathrm{d}x\mathrm{d}s\\&\quad+2\int_0^t\mathfrak{Re}\int_{\mathbb{R}}u(\mathrm{i}\varepsilon\bar{u})\mathrm{d}x\mathrm{d}W(s)+\int_0^t\mathfrak{Re}\int_{\mathbb{R}}\sum_{m\in\mathbb{N}}\varepsilon^2|u|^2(\phi e_m)^2\mathrm{d}x\mathrm{d}s\\&=\int_{\mathbb{R}}|u(0)|^2\mathrm{d}x.\end{aligned}$$

https://doi.org/10.4208/cicp.300815.180416a Published online by Cambridge University Press

The proof for $Q(v)$ is similar and thus we finish the proof. □

Remark 2.1. From the charge conservation laws (2.6), it is obvious that the system (1.2) conserves the total charge almost surely

$$\int_{\mathbb{R}}\Big(|u(x,t)|^2+|v(x,t)|^2\Big)\mathrm{d}x=\int_{\mathbb{R}}\Big(|u(x,0)|^2+|v(x,0)|^2\Big)\mathrm{d}x. \tag{2.7}$$

We now state the energy evolution law for CSNLS equations (1.2). To this end, we define the energy

$$H(u,v)=\int_{\mathbb{R}}\Big[\frac{\sigma}{4}(|u|^4+|v|^4)-\frac{\alpha}{2}(|u_x|^2+|v_x|^2)+\frac{\beta}{2}|u|^2|v|^2\Big]\mathrm{d}x. \tag{2.8}$$

Theorem 2.3. *The CSNLS equations* (1.2) *have the following global energy evolution law almost surely,*

$$\begin{aligned}H(u,v)=H(u_0,v_0)&-\alpha\varepsilon\int_0^t\mathfrak{Im}\int_{\mathbb{R}}\Big(u\bar{u}_x+v\bar{v}_x\Big)\mathrm{d}(\nabla W(s))\mathrm{d}x\\&-\frac{\alpha}{2}\varepsilon^2\sum_{k=1}^{\infty}\int_0^t\int_{\mathbb{R}}\Big(|u|^2+|v|^2\Big)|\nabla\phi e_k|^2\mathrm{d}x\mathrm{d}s,\end{aligned} \tag{2.9}$$

where $\mathfrak{Im}$, $\mathfrak{Re}$ *are the imaginary and real parts of a complex-valued function, respectively.*

Proof. To investigate the evolution relationship of the energy. We will apply Itô formula to the Hamiltonian $H(u,v)$. It is easy to verify that,

$$\begin{aligned}D_uH(u,v)(\psi)&=\mathfrak{Re}\Big(\int_{\mathbb{R}}(\sigma|u|^2+\beta|v|^2)\bar{u}\psi\mathrm{d}x-\alpha\int_{\mathbb{R}}\bar{u}_x\psi_x\mathrm{d}x\Big),\\D_vH(u,v)(\psi)&=\mathfrak{Re}\Big(\int_{\mathbb{R}}(\sigma|v|^2+\beta|u|^2)\bar{v}\psi\mathrm{d}x-\alpha\int_{\mathbb{R}}\bar{v}_x\psi_x\mathrm{d}x\Big),\\D^2_{u,u}H(u,v)(\psi,\phi)&=\mathfrak{Re}\Big(\int_{\mathbb{R}}(\sigma|u|^2+\beta|v|^2)\bar{\psi}\phi\mathrm{d}x-\alpha\int_{\mathbb{R}}\bar{\psi}_x\phi_x\mathrm{d}x\Big)\\&\quad+2\sigma\int_{\mathbb{R}}\mathfrak{Re}(\bar{u}\psi)\mathfrak{Re}(\bar{u}\phi)\mathrm{d}x,\\D^2_{v,v}H(u,v)(\psi,\phi)&=\mathfrak{Re}\Big(\int_{\mathbb{R}}(\sigma|v|^2+\beta|u|^2)\bar{\psi}\phi\mathrm{d}x-\alpha\int_{\mathbb{R}}\bar{\psi}_x\phi_x\mathrm{d}x\Big)\\&\quad+2\sigma\int_{\mathbb{R}}\mathfrak{Re}(\bar{v}\psi)\mathfrak{Re}(\bar{v}\phi)\mathrm{d}x,\\D^2_{u,v}H(u,v)(\psi,\phi)&=2\beta\int_{\mathbb{R}}\mathfrak{Re}(\bar{u}\psi)\mathfrak{Re}(\bar{v}\phi)\mathrm{d}x,\end{aligned} \tag{2.10}$$

where $D_uH(u,v)(\psi)$, $D^2_{u,v}H(u,v)(\psi,\phi)$ denote the first Fréchet derivative with respect to component u along direction ψ and the second Fréchet derivative with respect to components u,v along direction (ψ,ϕ), respectively.

https://doi.org/10.4208/cicp.300815.180416a Published online by Cambridge University Press

Based on the system (2.3), the Itô formula for $H(u,v)$ leads to

$$\begin{aligned}
\mathrm{d}H(u,v) =& D_u H(u)(\mathrm{d}u)+D_v H(v)(\mathrm{d}v)\\
&+\frac{1}{2}D^2_{u,u}H(u)(\mathrm{d}u,\mathrm{d}u)+D^2_{u,v}H(u,v)(\mathrm{d}u,\mathrm{d}v)+\frac{1}{2}D^2_{v,v}H(v)(\mathrm{d}v,\mathrm{d}v)\\
=&-\alpha\varepsilon\mathfrak{Im}\int_{\mathbb{R}}\Big(u\bar{u}_x+v\bar{v}_x\Big)\mathrm{d}(\nabla W(t))\mathrm{d}x\\
&+\frac{\alpha}{2}\varepsilon^2\underbrace{\mathfrak{Re}\int_{\mathbb{R}}\Big(\bar{u}_x\nabla(uF_\phi)+\bar{v}_x\nabla(vF_\phi)\Big)\mathrm{d}x\mathrm{d}t}_{A}\\
&-\frac{\alpha}{2}\varepsilon^2\underbrace{\sum_{k=1}^{\infty}\mathfrak{Re}\int_{\mathbb{R}}\Big(|\nabla(u\phi e_k)|^2+|\nabla(v\phi e_k)|^2\Big)\mathrm{d}x\mathrm{d}t}_{B}. \qquad (2.11)
\end{aligned}$$

After some simple algebraic manipulations, exploiting the definition of F_ϕ and integration by parts, we arrive at

$$A=\mathfrak{Re}\int_{\mathbb{R}}(|u_x|^2+|v_x|^2)F_\phi\mathrm{d}x\mathrm{d}t+2\sum_{k=1}^{\infty}\mathfrak{Re}\int_{\mathbb{R}}(u\bar{u}_x+v\bar{v}_x)(\phi e_k)\nabla(\phi e_k)\mathrm{d}x\mathrm{d}t,$$

and

$$\begin{aligned}
B=&\mathfrak{Re}\int_{\mathbb{R}}(|u_x|^2+|v_x|^2)F_\phi\mathrm{d}x\mathrm{d}t+2\sum_{k=1}^{\infty}\mathfrak{Re}\int_{\mathbb{R}}(u\bar{u}_x+v\bar{v}_x)(\phi e_k)\nabla(\phi e_k)\mathrm{d}x\mathrm{d}t\\
&+\sum_{k=1}^{\infty}\int_{\mathbb{R}}\Big(|u|^2+|v|^2\Big)|\nabla\phi e_k|^2\mathrm{d}x\mathrm{d}t.
\end{aligned}$$

Substituting the above equations into (2.11) and integrating the equation from 0 to t in temporal direction leads to (2.9). Thus the proof is finished. □

Remark 2.2. It follows from the proofs of Theorem 2.2 and Theorem 2.3, we can conclude that the charge conservation law and energy evolution law still hold for arbitrary number of CSNLS equations by some minor modifications.

3 A compact scheme for the CSNLS equations

We now propose the numerical scheme which we will use to simulate our stochastic equations (1.2) and, finally, we will state three conservation law theorems for this scheme.

The compact scheme which proposed in this paper behaves well: on one hand, it does not introduce any numerical dissipation and can simulate some important phenomena such as the evolution of a single soliton, the interaction of multi-solitons or the splitting of a profile into more solitons. On the other hand, it approximates to derivatives with fewer

https://doi.org/10.4208/cicp.300815.180416a Published online by Cambridge University Press

nodes and of higher accuracy, which is implemented by solving a tri-diagonal or a pent-diagonal linear algebraic system. The numerical experiments confirm all nice properties of the scheme. For more merits of the compact scheme in deterministic case, see [9, 11].

For simplicity, only homogeneous boundary condition is considered. The algorithms and conclusions described in this paper can be easily extended to the case of periodic boundary condition.

3.1 A compact scheme

Since storage of the solution requires to get a system of finite size, it seems natural to work on a bounded computational domain $[a, b]$. We introduce a uniform grid $(x_j,t_n)\in[a,b]\times[0,T]$ with mesh length h in the spatial direction and mesh length τ in the temporal direction, with $j=0,1,\cdots,J+1$, $n=0,1,\cdots,N+1$. The approximate value of the function $u(x,t)$ at the mesh point (x_j,t_n) is denoted by u_j^n. For convenience, we introduce the following operators

$$\delta_t u_j^n=\frac{u_j^{n+1}-u_j^n}{\tau},\quad \delta_x u_j^n=\frac{u_{j+1}^n-u_j^n}{h},\quad \delta_{x\bar{x}}u_j^n=\frac{u_{j+1}^n-2u_j^n+u_{j-1}^n}{h^2}$$

and two tridiagonal matrices

$$H=\frac{1}{12}\begin{pmatrix}10&1&&&\\1&10&1&&\\&\ddots&\ddots&\ddots&\\&&1&10&1\\&&&1&10\end{pmatrix}_{J\times J},\quad \mathcal{D}=\begin{pmatrix}2&-1&&&\\-1&2&-1&&\\&\ddots&\ddots&\ddots&\\&&-1&2&-1\\&&&-1&2\end{pmatrix}_{J\times J}.$$

With the definition of the above difference operators and matrices, the compact scheme for Eqs. (1.2) reads

$$\begin{aligned}&\mathrm{i}\delta_t\mathbf{u}^n+\alpha H^{-1}\delta_{x\bar{x}}\mathbf{u}^{n+\frac12}+\left(\sigma|\mathbf{u}^{n+\frac12}|^2+\beta|\mathbf{v}^{n+\frac12}|^2\right)\mathbf{u}^{n+\frac12}=\frac{\varepsilon}{\tau}\mathbf{u}^{n+\frac12}\Delta\mathbf{W}^n,\\&\mathrm{i}\delta_t\mathbf{v}^n+\alpha H^{-1}\delta_{x\bar{x}}\mathbf{v}^{n+\frac12}+\left(\sigma|\mathbf{v}^{n+\frac12}|^2+\beta|\mathbf{u}^{n+\frac12}|^2\right)\mathbf{v}^{n+\frac12}=\frac{\varepsilon}{\tau}\mathbf{v}^{n+\frac12}\Delta\mathbf{W}^n,\end{aligned}\tag{3.1}$$

where

$$\begin{aligned}&u_j^{n+\frac12}=\frac{u_j^{n+1}+u_j^n}{2},\quad \mathbf{u}^{n+\frac12}=\left[u_1^{n+\frac12},u_2^{n+\frac12},\cdots,u_J^{n+\frac12}\right]^T,\\&|\mathbf{u}^{n+\frac12}|^2\mathbf{v}^{n+\frac12}=\left[|u_1^{n+\frac12}|^2v_1^{n+\frac12},\,|u_2^{n+\frac12}|^2v_2^{n+\frac12},\,\cdots,\,|u_J^{n+\frac12}|^2v_J^{n+\frac12}\right]^T,\end{aligned}$$

and

$$\mathbf{u}^{n+\frac12}\Delta\mathbf{W}^n=\left[u_1^{n+\frac12}\Delta W_1^n,\,u_2^{n+\frac12}\Delta W_2^n,\,\cdots,\,u_J^{n+\frac12}\Delta W_J^n\right]^T.$$

https://doi.org/10.4208/cicp.300815.180416a Published online by Cambridge University Press

The random term can be simulated by

$$\Delta W_j^n = \frac{1}{h}\sqrt{\frac{2}{b-a}}\sum_{m=1}^{M}\int_{x_j}^{x_{j+1}} \sin\Big(\frac{m\pi(x-a)}{b-a}\Big)\mathrm{d}x\Big(\beta_m(t_{n+1})-\beta_m(t_n)\Big), \tag{3.2}$$

here, $(\beta_m(t_{n+1})-\beta_m(t_n))/\sqrt{\tau}$ are independent random variables with $\mathcal{N}(0,1)$ distribution.

Remark 3.1. In order to analyze the discrete stochastic multi-symplectic property, we rewrite the difference operator $\delta_{x\bar{x}}$ into the following form

$$\delta_{x\bar{x}}\mathbf{u}^{n+\frac{1}{2}} = -\frac{\mathcal{D}}{h^2}\mathbf{u}^{n+\frac{1}{2}}. \tag{3.3}$$

Remark 3.2. It is easy to verify that H and $\mathcal{D}$ are two symmetric and positive definite matrices.

Remark 3.3. In the case of periodic boundary condition, matrices H and $\mathcal{D}$ become

$$H=\frac{1}{12}\begin{pmatrix} 10 & 1 & & & 1\\ 1 & 10 & 1 & & \\ & \ddots & \ddots & \ddots & \\ & & 1 & 10 & 1\\ 1 & & & 1 & 10 \end{pmatrix}_{J\times J}, \quad \mathcal{D}=\begin{pmatrix} 2 & -1 & & & -1\\ -1 & 2 & -1 & & \\ & \ddots & \ddots & \ddots & \\ & & -1 & 2 & -1\\ -1 & & & -1 & 2 \end{pmatrix}_{J\times J}.$$

Furthermore, properties in Section 3 still hold for periodic boundary condition.

3.2 Properties of the compact scheme

In this subsection, we will analyze theoretically the discrete conservation properties for our compact scheme (3.1). Fist of all, we introduce two useful lemmas.

Lemma 3.1. *For symmetric and positive definite matrices H and $\mathcal{D}$, there exist unique symmetric and positive definite matrices $H^{\frac{1}{2}}$ and $\mathcal{D}^{\frac{1}{2}}$, such that $H=(H^{\frac{1}{2}})^2$, $\mathcal{D}=(\mathcal{D}^{\frac{1}{2}})^2$. Furthermore, we have $H\mathcal{D}=\mathcal{D}H$, $H\mathcal{D}^{\frac{1}{2}}=\mathcal{D}^{\frac{1}{2}}H$.*

Now the following lemma is obtained directly.

Lemma 3.2. *For symmetric and positive definite matrix H, we have*

$$-\langle H\delta_{x\bar{x}}\mathbf{u}^{n+\frac{1}{2}}, \mathbf{u}^{n+\frac{1}{2}}\rangle \geq 0, \tag{3.4}$$

and

$$-2\mathfrak{Re}\langle H\delta_{x\bar{x}}\mathbf{u}^{n+\frac{1}{2}}, \mathbf{u}^{n+1}-\mathbf{u}^n\rangle = |H^{\frac{1}{2}}\mathbf{u}^{n+1}|_1^2 - |H^{\frac{1}{2}}\mathbf{u}^n|_1^2, \tag{3.5}$$

with

$$\langle \mathbf{u}^n, \mathbf{v}^n\rangle = h\sum_{j=1}^{J} u_j^n\bar{v}_j^n, \quad |\mathbf{u}^n|_1^2 = h\sum_{j=1}^{J}|\mathcal{D}^{\frac{1}{2}}u_j^n|^2.$$

https://doi.org/10.4208/cicp.300815.180416a Published online by Cambridge University Press

3.2.1 Discrete stochastic multi-symplectic conservation law

Based on Lemma 3.1 and introducing new variables $\mathbf{a}=\mathcal{D}^{\frac{1}{2}}\mathbf{s}_1$, $\mathbf{b}=\mathcal{D}^{\frac{1}{2}}\mathbf{r}_1$, $\mathbf{c}=\mathcal{D}^{\frac{1}{2}}\mathbf{s}_2$, $\mathbf{d}=\mathcal{D}^{\frac{1}{2}}\mathbf{r}_2$, the compact scheme (3.1) can be written as the following first-order system

$$\begin{aligned}
&\delta_t\mathbf{r}_1^n-\frac{\alpha}{h^2}H^{-1}\mathcal{D}^{\frac{1}{2}}\mathbf{a}^{n+\frac{1}{2}}+(\sigma|\mathbf{u}^{n+\frac{1}{2}}|^2+\beta|\mathbf{v}^{n+\frac{1}{2}}|^2)\mathbf{s}_1^{n+\frac{1}{2}}=\frac{\varepsilon}{\tau}\mathbf{s}_1^{n+\frac{1}{2}}\Delta\mathbf{W}^n,\\
&\mathcal{D}^{\frac{1}{2}}\mathbf{s}_1^{n+\frac{1}{2}}=\mathbf{a}^{n+\frac{1}{2}},\\
&-\delta_t\mathbf{s}_1^n-\frac{\alpha}{h^2}H^{-1}\mathcal{D}^{\frac{1}{2}}\mathbf{b}^{n+\frac{1}{2}}+(\sigma|\mathbf{u}^{n+\frac{1}{2}}|^2+\beta|\mathbf{v}^{n+\frac{1}{2}}|^2)\mathbf{r}_1^{n+\frac{1}{2}}=\frac{\varepsilon}{\tau}\mathbf{r}_1^{n+\frac{1}{2}}\Delta\mathbf{W}^n,\\
&\mathcal{D}^{\frac{1}{2}}\mathbf{r}_1^{n+\frac{1}{2}}=\mathbf{b}^{n+\frac{1}{2}},\\
&\delta_t\mathbf{r}_2^n-\frac{\alpha}{h^2}H^{-1}\mathcal{D}^{\frac{1}{2}}\mathbf{c}^{n+\frac{1}{2}}+(\sigma|\mathbf{v}^{n+\frac{1}{2}}|^2+\beta|\mathbf{u}^{n+\frac{1}{2}}|^2)\mathbf{s}_2^{n+\frac{1}{2}}=\frac{\varepsilon}{\tau}\mathbf{s}_2^{n+\frac{1}{2}}\Delta\mathbf{W}^n,\\
&\mathcal{D}^{\frac{1}{2}}\mathbf{s}_2^{n+\frac{1}{2}}=\mathbf{c}^{n+\frac{1}{2}},\\
&-\delta_t\mathbf{s}_2^n-\frac{\alpha}{h^2}H^{-1}\mathcal{D}^{\frac{1}{2}}\mathbf{d}^{n+\frac{1}{2}}+(\sigma|\mathbf{v}^{n+\frac{1}{2}}|^2+\beta|\mathbf{u}^{n+\frac{1}{2}}|^2)\mathbf{r}_2^{n+\frac{1}{2}}=\frac{\varepsilon}{\tau}\mathbf{r}_2^{n+\frac{1}{2}}\Delta\mathbf{W}^n,\\
&\mathcal{D}^{\frac{1}{2}}\mathbf{r}_2^{n+\frac{1}{2}}=\mathbf{d}^{n+\frac{1}{2}}.
\end{aligned}\tag{3.6}$$

Let $\mathbf{Z}=(\mathbf{r}_1^T,\mathbf{s}_1^T,\mathbf{r}_2^T,\mathbf{s}_2^T,\mathbf{a}^T,\mathbf{b}^T,\mathbf{c}^T,\mathbf{d}^T)^T$, we can write Eqs. (3.6) into stochastic multi-symplectic framework

$$\mathbb{K}\delta_t\mathbf{Z}^n+\frac{1}{h^2}\mathbb{L}\mathbb{D}\mathbf{Z}^{n+\frac{1}{2}}=\nabla_{\mathbf{Z}}\tilde{S}_1(\mathbf{Z}^{n+\frac{1}{2}})+\nabla_{\mathbf{Z}}\tilde{S}_2(\mathbf{Z}^{n+\frac{1}{2}})\frac{\Delta\mathbf{W}^n}{\tau},\quad \mathbf{Z}\in\mathbb{R}^{8J},\tag{3.7}$$

where

$$\begin{aligned}
\tilde{S}_1(\mathbf{Z})=&\frac{\sigma}{4}\Big[(|\mathbf{r}_1|^2+|\mathbf{s}_1|^2)^2+(|\mathbf{r}_2|^2+|\mathbf{s}_2|^2)^2\Big]+\frac{\beta}{2}(|\mathbf{r}_1|^2+|\mathbf{s}_1|^2)(|\mathbf{r}_2|^2+|\mathbf{s}_2|^2)\\
&+\frac{\alpha}{2}\Big(\mathbf{a}^TH^{-1}\mathbf{a}+\mathbf{b}^TH^{-1}\mathbf{b}+\mathbf{c}^TH^{-1}\mathbf{c}+\mathbf{d}^TH^{-1}\mathbf{d}\Big),\\
\tilde{S}_2(\mathbf{Z})=&-\frac{\varepsilon}{2}\Big(|\mathbf{r}_1|^2+|\mathbf{s}_1|^2+|\mathbf{r}_2|^2+|\mathbf{s}_2|^2\Big),
\end{aligned}$$

and

$$\mathbb{K}=\begin{pmatrix}\text{Æ}&\mathbf{0}\\ \mathbf{0}&\mathbf{0}\end{pmatrix}_{8J\times 8J},\quad \mathbb{L}=\begin{pmatrix}\mathbf{0}&-\text{Œ}\\ \text{Œ}&\mathbf{0}\end{pmatrix}_{8J\times 8J},\quad \mathbb{D}=\begin{pmatrix}\mathcal{D}^{\frac{1}{2}}&&\\ &\ddots&\\ &&\mathcal{D}^{\frac{1}{2}}\end{pmatrix}_{8J\times 8J}$$

with

$$\text{Æ}=\begin{pmatrix}\mathbf{0}&I&\mathbf{0}&\mathbf{0}\\ -I&\mathbf{0}&\mathbf{0}&\mathbf{0}\\ \mathbf{0}&\mathbf{0}&\mathbf{0}&I\\ \mathbf{0}&\mathbf{0}&-I&\mathbf{0}\end{pmatrix}_{4J\times 4J},\quad \text{Œ}=\begin{pmatrix}\mathbf{0}&-\alpha H^{-1}&\mathbf{0}&\mathbf{0}\\ -\alpha H^{-1}&\mathbf{0}&\mathbf{0}&\mathbf{0}\\ \mathbf{0}&\mathbf{0}&\mathbf{0}&-\alpha H^{-1}\\ \mathbf{0}&\mathbf{0}&-\alpha H^{-1}&\mathbf{0}\end{pmatrix}_{4J\times 4J}.$$

https://doi.org/10.4208/cicp.300815.180416a Published online by Cambridge University Press

The variational equation for Eq. (3.7) reads

$$\mathbb{K}\delta_t \mathrm{d}\mathbf{Z}^n + \frac{1}{h^2}\mathbb{L}\mathbb{D}\mathrm{d}\mathbf{Z}^{n+\frac{1}{2}} = \nabla^2_{\mathbf{Z}}\tilde{S}_1(\mathbf{Z}^{n+\frac{1}{2}})\mathrm{d}\mathbf{Z}^{n+\frac{1}{2}} + \nabla^2_{\mathbf{Z}}\tilde{S}_2(\mathbf{Z}^{n+\frac{1}{2}})\mathrm{d}\mathbf{Z}^{n+\frac{1}{2}}\frac{\Delta \mathbf{W}^n}{\tau}. \tag{3.8}$$

Taking the wedge product with $\mathrm{d}\mathbf{Z}^{n+\frac{1}{2}}$, we can obtain

$$\frac{\mathrm{d}\mathbf{Z}^{n+1}\wedge\mathbb{K}\mathrm{d}\mathbf{Z}^{n+1} - \mathrm{d}\mathbf{Z}^n\wedge\mathbb{K}\mathrm{d}\mathbf{Z}^n}{2\tau} + \frac{1}{h^2}\mathrm{d}\mathbf{Z}^{n+\frac{1}{2}}\wedge\mathbb{L}\mathbb{D}\mathrm{d}\mathbf{Z}^{n+\frac{1}{2}} = 0,$$

where we use $\mathrm{d}\mathbf{Z}^{n+\frac{1}{2}} = \frac{1}{2}\big(\mathrm{d}\mathbf{Z}^{n+1} + \mathrm{d}\mathbf{Z}^n\big)$ and the following properties of differential 2-forms: let ξ,η be n-dimensional differential 1-forms and M be an $n\times n$ matrix, we have

$$\xi\wedge M\eta = M^T\xi\wedge\eta, \qquad \xi\wedge\eta = -\eta\wedge\xi.$$

Consequently, one obtains the following theorem:

Theorem 3.1. *The compact scheme* (3.1) *has the following discrete stochastic multi-symplectic conservation law almost surely*

$$\frac{\omega^{n+1}-\omega^n}{\tau} + \frac{1}{h^2}\mathrm{d}\mathbf{Z}^{n+\frac{1}{2}}\wedge\mathbb{L}\mathbb{D}\mathrm{d}\mathbf{Z}^{n+\frac{1}{2}} = 0, \tag{3.9}$$

where $\omega^n = \frac{1}{2}\mathrm{d}\mathbf{Z}^n\wedge\mathbb{K}\mathrm{d}\mathbf{Z}^n$.

3.2.2 Discrete charge conservation law

Next, we are interested in the discrete charge conservation law for the compact scheme (3.1).

Theorem 3.2. *Under the homogeneous boundary condition, the compact scheme* (3.1) *possesses the discrete charge conservation law almost surely, i.e.,*

$$h\sum_{j=1}^{J}|u_j^{n+1}|^2 = h\sum_{j=1}^{J}|u_j^n|^2, \ \ h\sum_{j=1}^{J}|v_j^{n+1}|^2 = h\sum_{j=1}^{J}|v_j^n|^2. \tag{3.10}$$

Proof. We multiply both sides of the first equation of system (3.1) by $2\bar{\mathbf{u}}^{n+\frac{1}{2}}$, which is the conjugate of $2\mathbf{u}^{n+\frac{1}{2}}$, and taking the imaginary part, it yields

$$\mathfrak{Re}\langle\delta_t\mathbf{u}^n, 2\mathbf{u}^{n+\frac{1}{2}}\rangle + \alpha\mathfrak{Im}\langle H^{-1}\delta_{x\bar{x}}\mathbf{u}^{n+\frac{1}{2}}, 2\mathbf{u}^{n+\frac{1}{2}}\rangle = 0, \tag{3.11}$$

where the equality is due to the real-valued of Wiener process $W(t)$.

It follows from Lemma 3.2, we have $\langle H^{-1}\delta_{x\bar{x}}\mathbf{u}^{n+\frac{1}{2}}, 2\mathbf{u}^{n+\frac{1}{2}}\rangle \in \mathbb{R}$. Combining all these equalities and the definition of differential operators, we can get the first result of (3.10). Analogously, one can get the result of v. Thus the proof is finished. □

Remark 3.4. Theorem 3.2 implies that the compact scheme (3.1) is unitary. It also implies that the compact scheme maintains the total charge conservation, that is,

$$h\sum_{j=1}^{J}\Big(|u_j^{n+1}|^2 + |v_j^{n+1}|^2\Big) = h\sum_{j=1}^{J}\Big(|u_j^n|^2 + |v_j^n|^2\Big).$$

https://doi.org/10.4208/cicp.300815.180416a Published online by Cambridge University Press

3.2.3 Discrete energy evolution law

The next result concerns the error estimation of the discrete global energy of the compact scheme.

Theorem 3.3. *Under the homogeneous boundary condition, the compact scheme* (3.1) *has the following recursion of discrete global energy conservation law, i.e.,*

$$\mathcal{H}^{n+1}=\mathcal{H}^n+\frac{\varepsilon h}{2\tau}\sum_{j=1}^{J}\Big(|u_j^{n+1}|^2+|v_j^{n+1}|^2-|u_j^n|^2-|v_j^n|^2\Big)\Delta W_j^n. \tag{3.12}$$

Here, the discrete global energy of the scheme (3.1) *at time t_n is defined as*

$$\mathcal{H}^n=-\frac{\alpha}{2}\Big(|H^{-\frac{1}{2}}\mathbf{u}^n|_1^2+|H^{-\frac{1}{2}}\mathbf{v}^n|_1^2\Big)+\frac{h\sigma}{4}\sum_{j=1}^{J}\Big(|u_j^n|^4+|v_j^n|^4\Big)+\frac{h\beta}{2}\sum_{j=1}^{J}|u_j^n|^2|v_j^n|^2.$$

Proof. Multiplying both sides of Eqs. (3.1) by $\tau\delta_t\bar{\mathbf{u}}^n$, $\tau\delta_t\bar{\mathbf{v}}^n$, then taking the real part, by Lemma 3.2, it yields

$$\begin{aligned}&-\frac{\alpha}{2}\Big(|H^{-\frac{1}{2}}\mathbf{u}^{n+1}|_1^2-|H^{-\frac{1}{2}}\mathbf{u}^n|_1^2\Big)+\frac{h\sigma}{4}\sum_{j=1}^{J}\Big(|u_j^{n+1}|^4-|u_j^n|^4\Big)\\&+\frac{h\beta}{4}\sum_{j=1}^{J}\Big(|u_j^{n+1}|^2-|u_j^n|^2\Big)\Big(|v_j^{n+1}|^2+|v_j^n|^2\Big)=\frac{h\varepsilon}{2\tau}\sum_{j=1}^{J}\Big(|u_j^{n+1}|^2-|u_j^n|^2\Big)\Delta W_j^n,\end{aligned} \tag{3.13}$$

and

$$\begin{aligned}&-\frac{\alpha}{2}\Big(|H^{-\frac{1}{2}}\mathbf{v}^{n+1}|_1^2-|H^{-\frac{1}{2}}\mathbf{v}^n|_1^2\Big)+\frac{h\sigma}{4}\sum_{j=1}^{J}\Big(|v_j^{n+1}|^4-|v_j^n|^4\Big)\\&+\frac{h\beta}{4}\sum_{j=1}^{J}\Big(|v_j^{n+1}|^2-|v_j^n|^2\Big)\Big(|u_j^{n+1}|^2+|u_j^n|^2\Big)=\frac{h\varepsilon}{2\tau}\sum_{j=1}^{J}\Big(|v_j^{n+1}|^2-|v_j^n|^2\Big)\Delta W_j^n.\end{aligned} \tag{3.14}$$

Since,

$$\begin{aligned}&\Big(|u_j^{n+1}|^2-|u_j^n|^2\Big)\Big(|v_j^{n+1}|^2+|v_j^n|^2\Big)+\Big(|v_j^{n+1}|^2-|v_j^n|^2\Big)\Big(|u_j^{n+1}|^2+|u_j^n|^2\Big)\\&=2\Big(|u_j^{n+1}|^2|v_j^{n+1}|^2-|u_j^n|^2|v_j^n|^2\Big),\end{aligned}$$

and adding (3.13) to (3.14), we then have the transformation of the global energy (3.12). Thus the proof is finished. □

https://doi.org/10.4208/cicp.300815.180416a Published online by Cambridge University Press

4 Results and discussion

In this section, we will present some detailed numerical investigations of CSNLS equations based on the compact scheme. In particular, we will focus on the conservation laws and the random potential effects on solitons. Furthermore, we check the temporal accuracy by fixing the space step sufficiently small such that errors stemming from the spatial approximation are negligible.

4.1 Evolution of a single soliton

In order to investigate the influence on the evolution of a single soliton in the presence of a random potential, we choose a soliton profile as the initial data to solve Eqs. (1.2),

$$\begin{aligned} u(x,0) &= \sqrt{\frac{2\gamma}{1+\beta}}\,\mathrm{sech}(\sqrt{2\gamma}x)\exp(\mathrm{i}cx), \\ v(x,0) &= -\sqrt{\frac{2\gamma}{1+\beta}}\,\mathrm{sech}(\sqrt{2\gamma}x)\exp(\mathrm{i}cx), \end{aligned} \tag{4.1}$$

where γ, β and c are constants. In this subsection, we choose parameters as $\alpha=0.5$, $\sigma=1$, $\beta=2/3$, $\gamma=1$, $c=1$.

In the following experiments, we take the temporal step-size $\tau=0.01$, the spatial meshgrid-size $h=0.1$, and the time interval $[0,100]$, the numerical spatial domain $[a,b]=[-20,100]$.

As is stated in Theorem 3.2, the compact scheme (3.1) could preserve the discrete charge conservation law almost surely. We consider this phenomenon numerically in Fig. 1, where the left one shows the evolution of the discrete charge conservation law and the right one is about the global error in the case of ε=0.01, 0.05 and 0.10. Although different sizes of noise are chosen, the figures of the discrete charge conservation law remain to be horizontal lines approximately, and the global residuals of the discrete charge conservation law all reach the magnitude of 10^{-11} for various ε. We observe a good agreement with the theoretical result.

Remark 4.1. According to Theorem 2.3, the averaged energy $\mathbb{E}(H(u,v))$ of the CSNLS equations (1.2) satisfies the following equality:

$$\mathbb{E}(H(u,v))=\mathbb{E}(H(u_0,v_0))-\frac{\alpha}{2}\varepsilon^2\mathbb{E}\sum_{k=1}^{\infty}\int_0^t\int_{\mathbb{R}}\left(|u|^2+|v|^2\right)|\nabla\phi e_k|^2\mathrm{d}x\mathrm{d}s. \tag{4.2}$$

It can be easily observed from (4.2) that, the averaged energy $\mathbb{E}(H(u,v))$ follows a dissipative evolution law. This phenomena is reflected in Fig. 2, where the evolution of the averaged discrete energy decays linearly over 100 trajectories, and so is the discrete energy for one trajectory with various ε.

https://doi.org/10.4208/cicp.300815.180416a Published online by Cambridge University Press

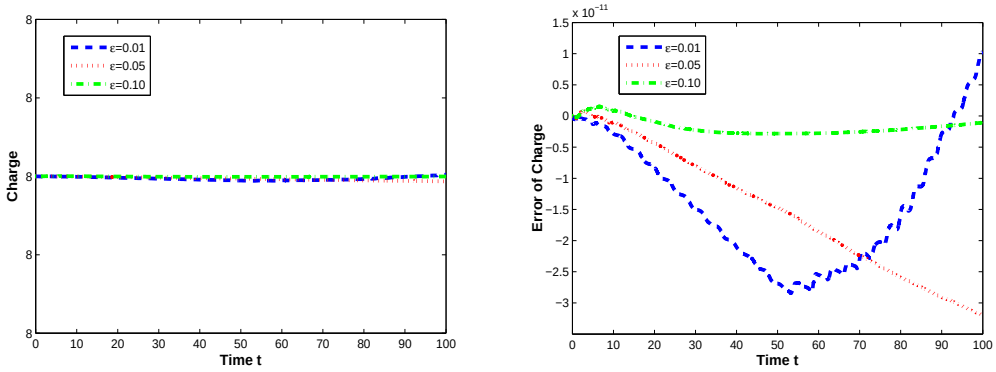


Figure 1: Evolution of the discrete charge conservation law (left), and the global errors of the discrete charge conservation law (right), as $\varepsilon = 0.01,\ 0.05,\ 0.10$.

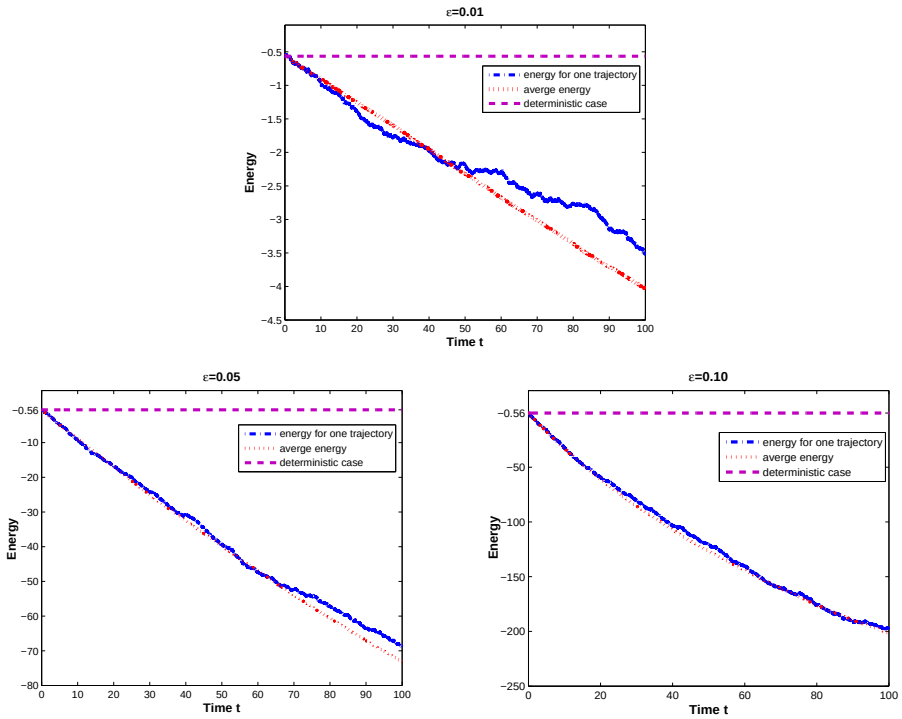


Figure 2: Evolution of average discrete energy along 100 trajectories and discrete energy over one trajectory as $\varepsilon = 0.01,\ 0.05,\ 0.10$.

We run the following experiments with different amplitudes of noise for the component u. Fig. 3 plots the influence of noise on the soliton profile at different instants in the case of $\varepsilon = 0.01$, where the red and green lines represent two samples of the profiles, and the black line denotes the profile for the deterministic problem. It seems that the soliton

https://doi.org/10.4208/cicp.300815.180416a Published online by Cambridge University Press

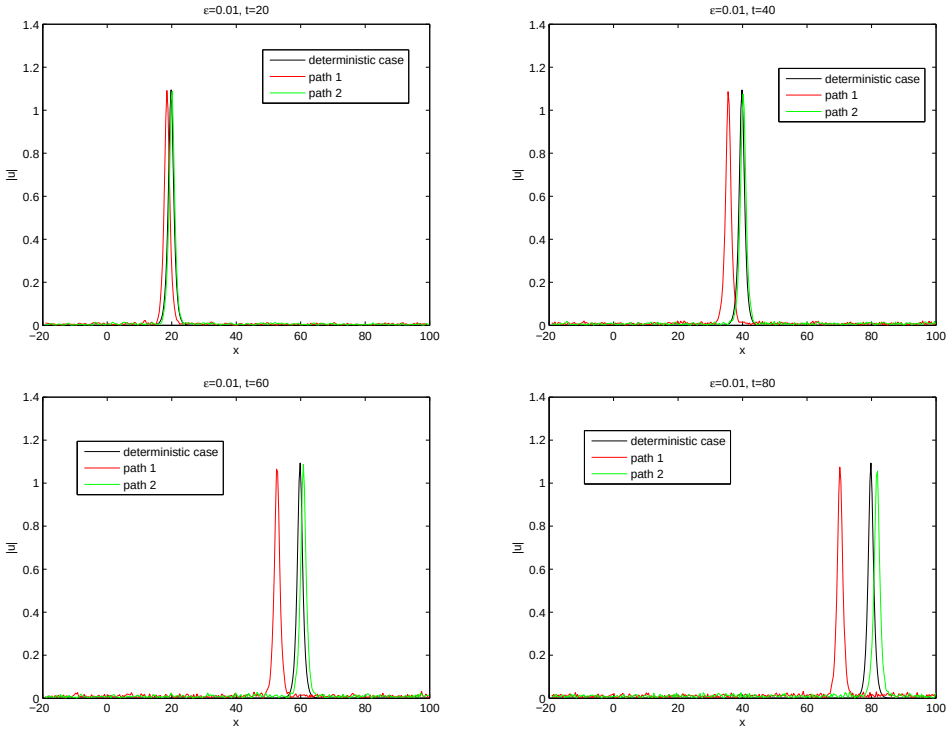


Figure 3: Shift of profiles of $|u|$ at different time with $\varepsilon=0.01$.

does not seem to be strongly perturbed in the short propagation interval. When the time becomes larger, we can see a significant shift of the profiles, but the shape of the profile does not present obvious changes. Taking path 1 (the red line of the plot) as an example, we see that at $t=20$, the shape of the soliton profile does not present obvious change; at $t=40$, the position of the peak is around $x=37$; at $t=60$, it is around $x=55$; at $t=80$, the position of the peak is about at $x=73$. Moreover, we could observe a slight modification of amplitudes of profiles in the presence of noise. And the noise may introduce oscillations to the profiles of the soliton, and the amplitude of oscillations is negligible if compared with the amplitudes of the soliton.

In order to further investigate the profiles of the soliton under the influence of noise, we increase the amplitude of the noise to $\varepsilon=0.05$, 0.10. In Fig. 4, with $\varepsilon=0.05$, we see that, indeed, the noise introduces much stronger perturbations and the phase shift is sensibly modified by the noise. Furthermore, the amplitude of the soliton decays with respect to time. However, we can see that the soliton is not totally destroyed. The evolution of the soliton in the case of $\varepsilon=0.10$ is shown in Fig. 5 at $t=20$, 40, 60 and 80. Under the influence of big sizes of noise, the amplitude of soliton is much smaller than that in the deterministic case; see the case of $t=20$, but we can still identify the shape of the soliton. For large $t=40$, 60, 80, we can no longer recognize the soliton and it is totally destroyed.

https://doi.org/10.4208/cicp.300815.180416a Published online by Cambridge University Press

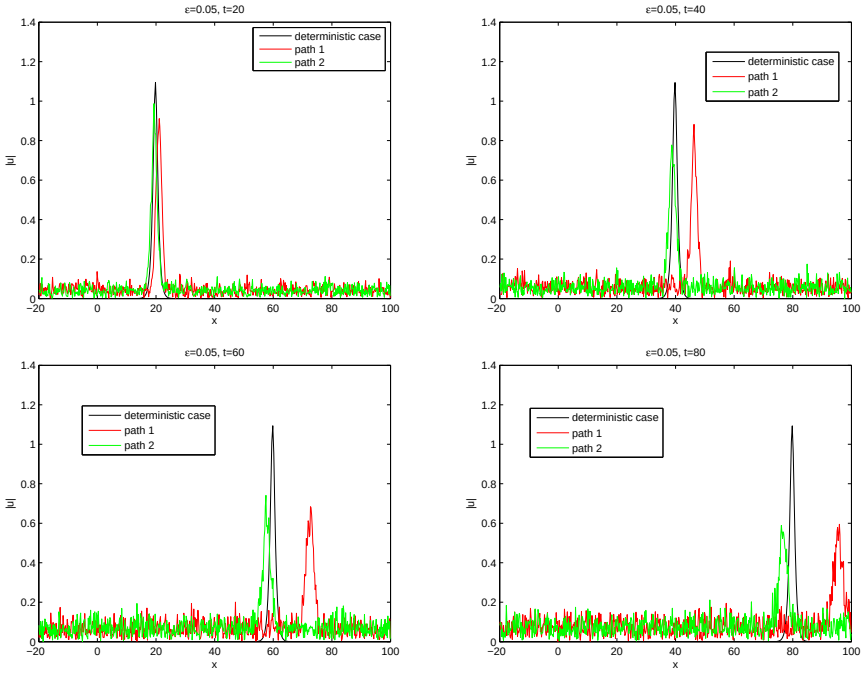


Figure 4: Shift of profiles of $|u|$ at different time with $\varepsilon = 0.05$.

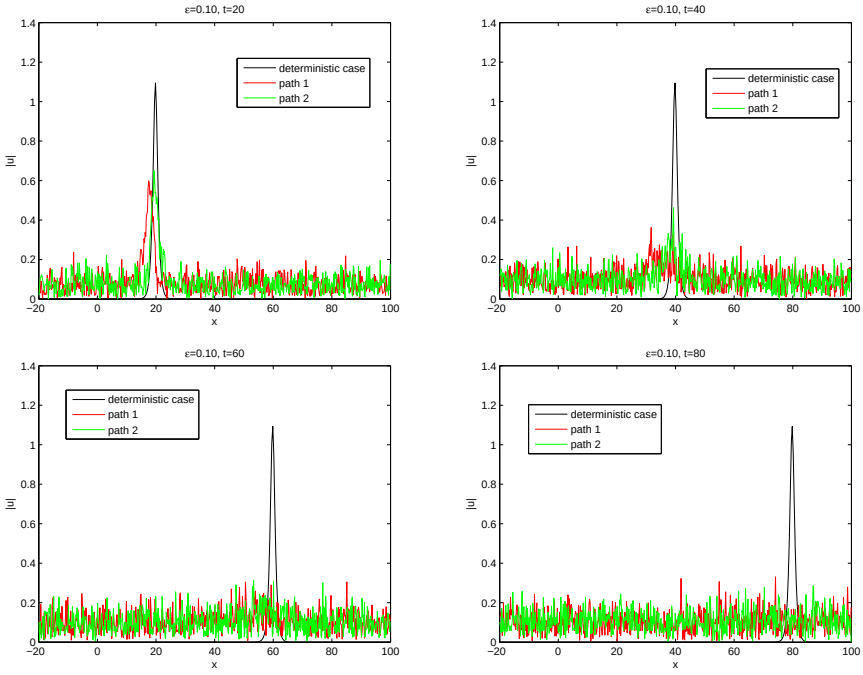


Figure 5: Shift of profiles of $|u|$ at different time with $\varepsilon = 0.10$.

https://doi.org/10.4208/cicp.300815.180416a Published online by Cambridge University Press

The above phenomena are similar to the observations in [2] that the small noise does not perturb the soliton strongly and does not prevent the propagation while high level noise could destroy the wave. It indicates that the noise introduces oscillations to the profiles and could create new waves, and these waves interact with the original solitary wave, which is inelastic interactions, leading to the decrease of the amplitude of the profile, i.e., the decay of the solitary wave.

4.2 Collision of two solitons

The next step is to simulate the collision of two solitons. The initial data are

$$u(x,0)=\sqrt{\frac{2\alpha_1}{1+\beta}}\text{sech}(\sqrt{2\gamma}x)\exp(\text{i}c_1x)+\sqrt{\frac{2\alpha_2}{1+\beta}}\text{sech}(\sqrt{2\alpha_1}(x-x_0))\exp(\text{i}c_2(x-\delta)),$$

and

$$v(x,0)=-\sqrt{\frac{2\alpha_1}{1+\beta}}\text{sech}(\sqrt{2\gamma}x)\exp(\text{i}c_1x)-\sqrt{\frac{2\alpha_2}{1+\beta}}\text{sech}(\sqrt{2\alpha_1}(x-x_0))\exp(\text{i}c_2(x-\delta)),$$

where $a=-20$, $b=150$, $T=60$, $\alpha=0.5$, $\beta=2/3$, $\gamma=1$ $\alpha_1=1$, $\alpha_2=0.5$, $c_1=2$, $c_2=0.5$, $\delta=30$.

Since the module of u is identical to v, we only provide surfaces of $|u|$. The intensity profiles and contours of solitons with various sizes of noise $\varepsilon=0.01$, 0.05, 0.10 for one trajectory are shown in Figs. 6-7. When the noise amplitude is small, $\varepsilon=0.01$, the soliton does not seem to be strongly perturbed. However, when the noise amplitude becomes larger, $\varepsilon=0.05$, we observe that the noise introduces much stronger perturbations. Their amplitudes become smaller. In particular, when $\varepsilon=0.10$, the soliton is almost collapsed. These observations recover some of those in Subsection 4.1. We pay more attention to the case $\varepsilon=0.10$. At the beginning there are two solitons with different amplitudes, and let us label the one with bigger amplitude *Soliton-I* and the other one *Soliton-II*. As we can see from the right bottom figure in Fig. 7, the evolution of *Soliton-II* almost stops after their interaction while *Soliton-I* propagates for much longer time. It seems that the soliton with larger amplitude may propagate for longer time.

We focus on the interaction of solitons in this subsection, as we can see from the initial data that it is composed by two profiles of solitons. In Figs. 8-10, we plot the interaction profiles at time $t=0$, 15, 21 and 60 for different sizes of noise $\varepsilon=0.01$, 0.05, 0.10. From Fig. 8 with $\varepsilon=0.01$, we notice that the influence of noise imposed on the solitons is almost ignorable in short time interval, e.g., [0,21]. When time increases to $t=60$, there is an apparent shift of solitons similar to the case of the evolution of a single soliton. And we can see that the noise introduces some oscillations to the solitons, especially to *Soliton-II*; it can be seen again in the case $\varepsilon=0.05$ (Fig. 9) that *Soliton-II* is about to be covered by waves introduced by the noise while the shape of *Soliton-I* could still be identified at time $t=60$ with damped amplitude. In the case $\varepsilon=0.10$, the oscillation generated by the noise

https://doi.org/10.4208/cicp.300815.180416a Published online by Cambridge University Press

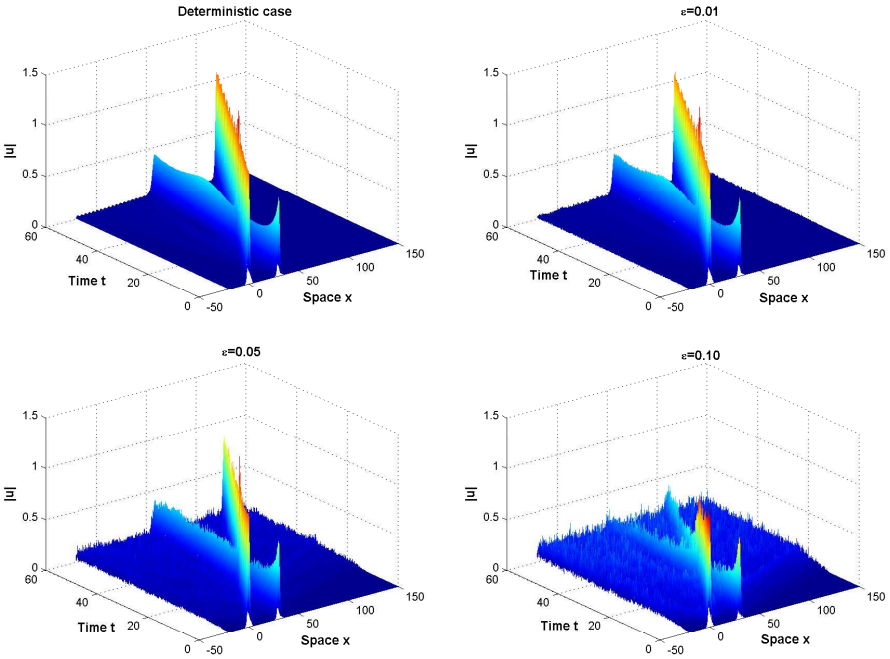


Figure 6: Intensity profiles of solitons along one trajectory.

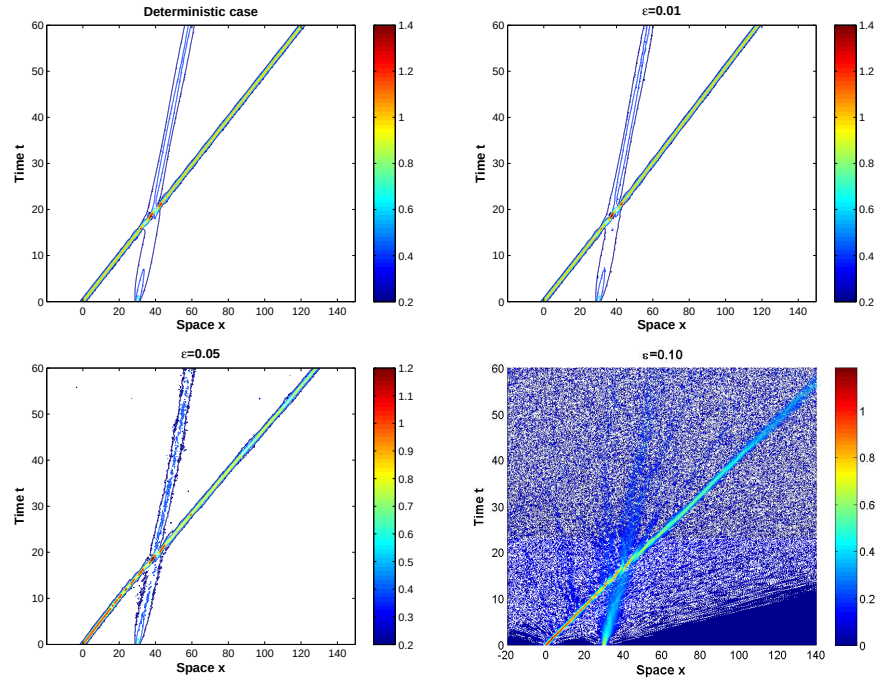


Figure 7: Intensity contours of two solitons along one trajectory.

https://doi.org/10.4208/cicp.300815.180416a Published online by Cambridge University Press

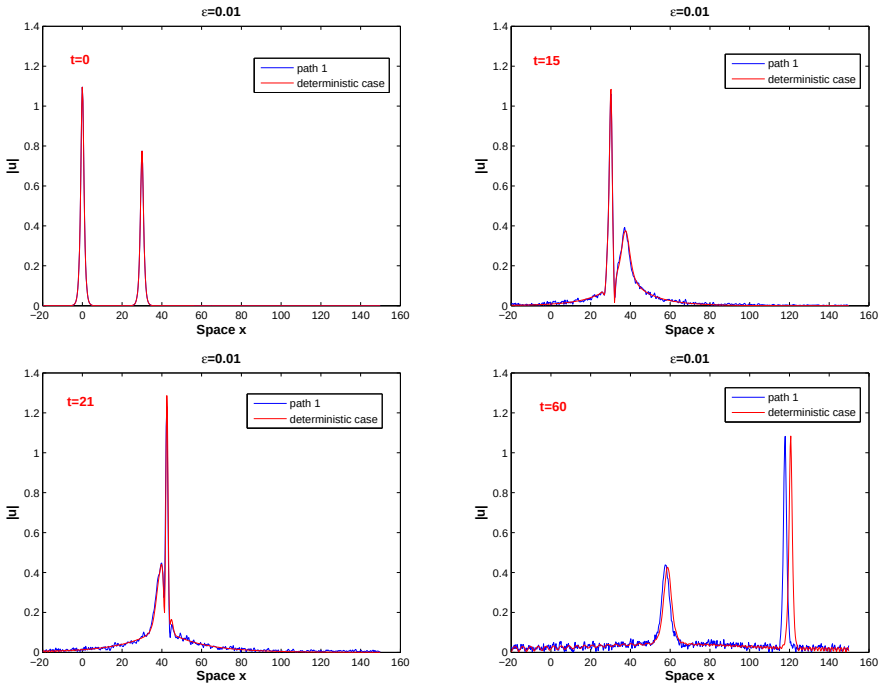


Figure 8: Collision of two solitons along one trajectory with $\varepsilon = 0.01$.

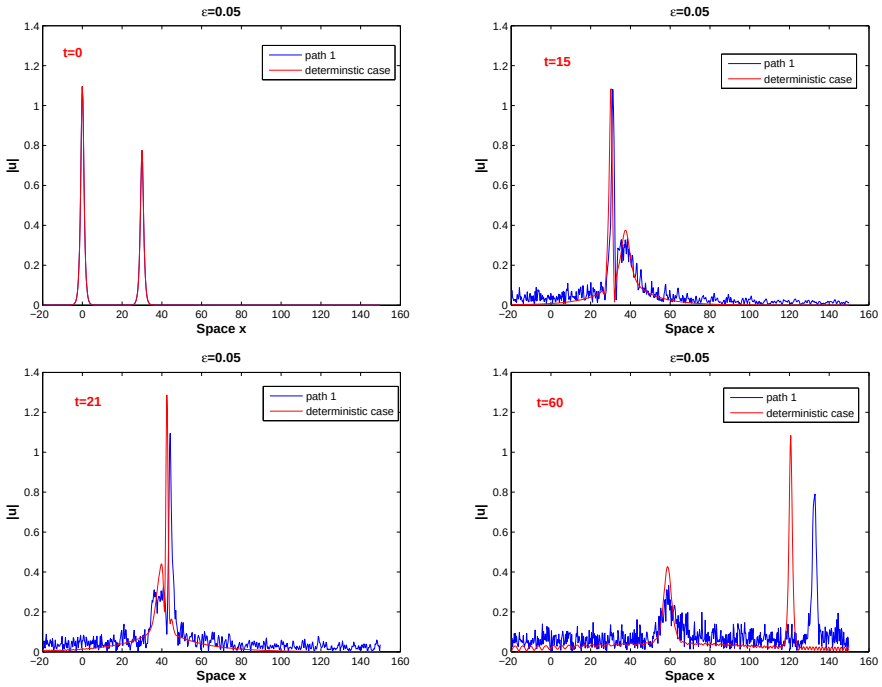


Figure 9: Collision of two solitons along one trajectory with $\varepsilon = 0.05$.

https://doi.org/10.4208/cicp.300815.180416a Published online by Cambridge University Press

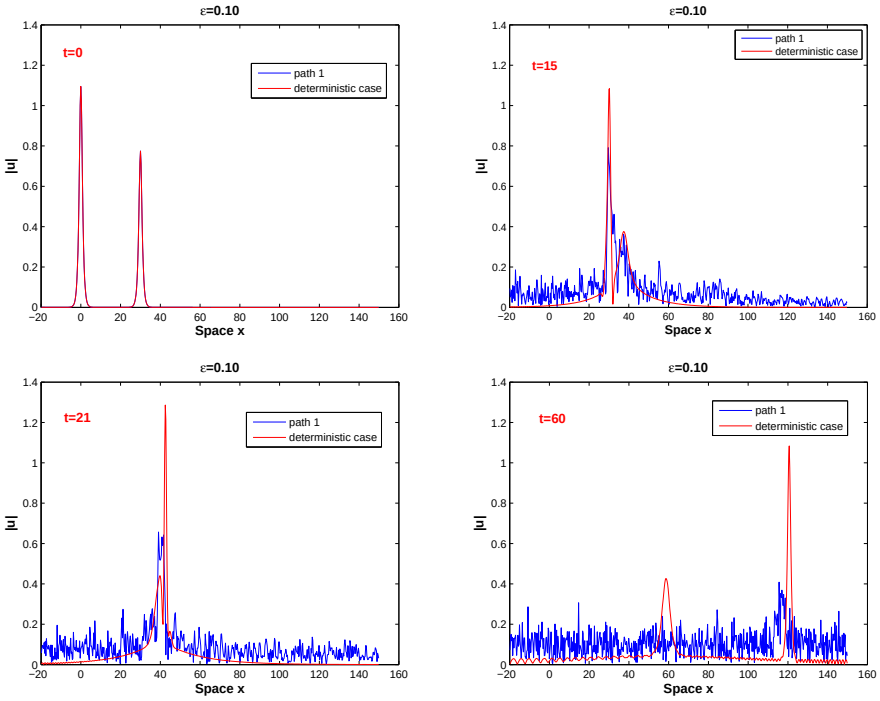


Figure 10: Collision of two solitons along one trajectory with $\varepsilon = 0.10$.

is much stronger and it accelerates the decay of the soliton amplitude; we can no longer identify the shape of *Soliton-I* at the time $t = 60$.

From these figures, we can observe that an elastic (i.e., shape unchanging) soliton collision between two solitons is illustrated in the deterministic case. However, when the noise amplitude increases, the figures present inelastic interaction (i.e., shaping changing) with a significant shift of the peak. And the elasticity property of the collision is destroyed by the noise. We may then say that the noise is responsible for the possible destruction of the soliton.

4.3 Reflexionless potential case

To study the influence of noise on the splitting of a profile into more solitons, the third test we performed is the evolution of the following initial values

$$\begin{aligned} u(x,0) &= \sqrt{2} r_1 \operatorname{sech}\left(r_1 x + \frac{1}{2} D_0\right) \exp(\mathrm{i} V_0 x/4), \\ v(x,0) &= \sqrt{2} r_2 \operatorname{sech}\left(r_2 x + \frac{1}{2} D_0\right) \exp(-\mathrm{i} V_0 x/4), \end{aligned} \tag{4.3}$$

https://doi.org/10.4208/cicp.300815.180416a Published online by Cambridge University Press

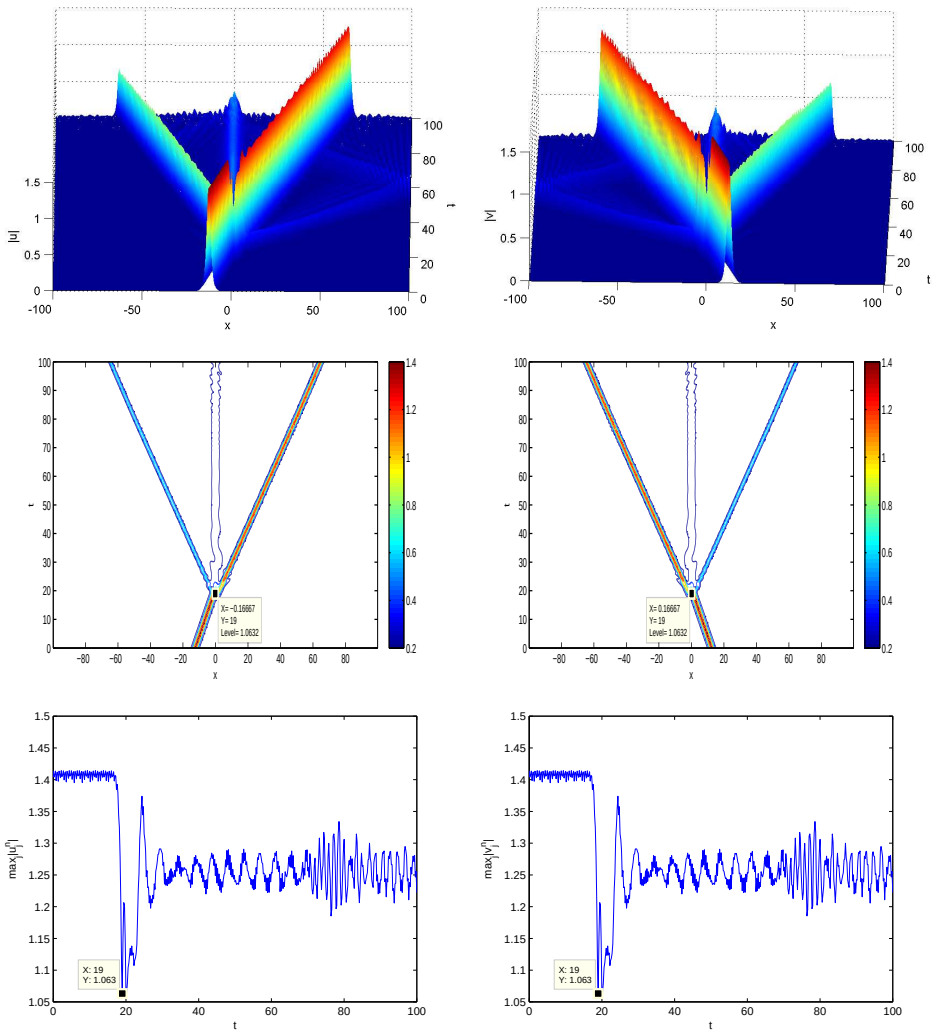


Figure 11: Splitting of the reflexionless potential profile for $\varepsilon=0.01$ (Left: $|u|$; Right: $|v|$).

where r_1, r_2, D_0 and V_0 are constants. We choose the following parameters:

$$a=-100,\ b=100,\ T=100,\ \alpha=1,\ \sigma=1,$$
$$\beta=2/3,\ r_1=r_2=1,\ D_0=25,\ V_0=1.20757148.$$

As is shown in [1], the inverse scattering method shows that this profile splits into several solitary waves with no dispersive tail. The evolutions of $|u|$ and $|v|$, the contours and the maximum modules are shown in Fig. 11. From this figure, we may make a rough guess that for deterministic CNLS equations (1.1), the time of creation of new waves for components u and v is about $t=19$, and the modulus of u and v equal to $|u|=|v|=1.0632$.

https://doi.org/10.4208/cicp.300815.180416a Published online by Cambridge University Press

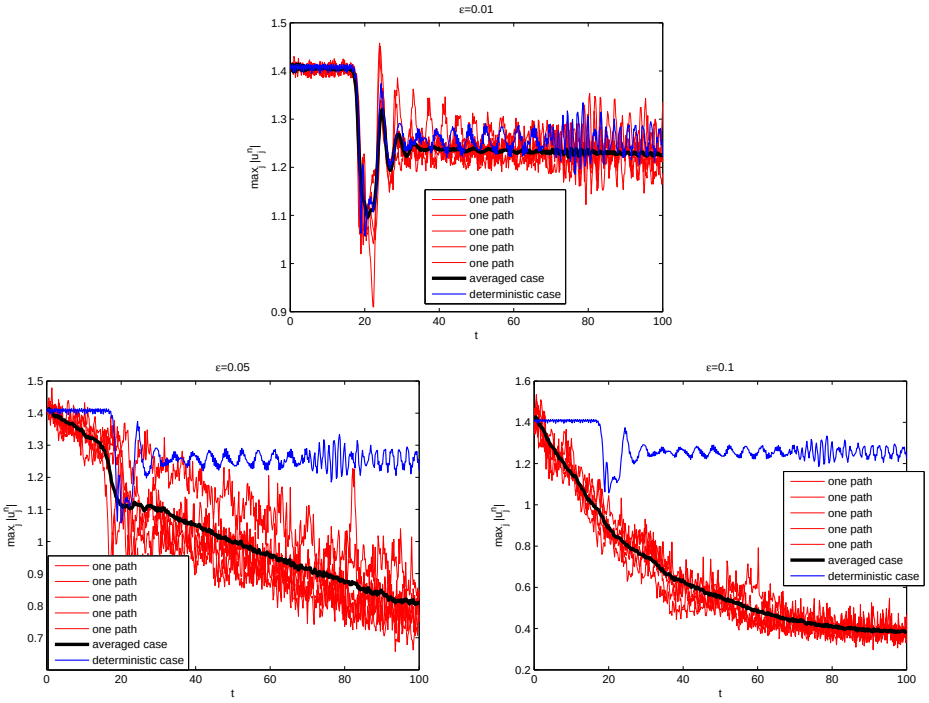


Figure 12: Maximum modules of u with different sizes of noise $\varepsilon=0.01,\ 0.05,\ 0.10$.

We are also interested in the behavior of the maximum modules of components u and v. Fig. 12 plots the maximum modules of u for different amplitudes of noise. The black line represents the averaged value over 100 trajectories, the red lines are five samples, and the blue one is for deterministic case. For the case $\varepsilon=0.01$, the behavior of the averaged value is close to but is smoother than that of deterministic case. As the increase of the amplitude of noise $(\varepsilon=0.05$ or $0.10)$, the behavior of the averaged value separates from the deterministic one, and shows us a smooth and steady decrease. The larger the amplitude of noise is, the smaller the averaged value at the final time $t=100$ be.

4.4 Random effect to N-coupled case

In this subsection, we will numerically investigate the random effect to the soliton evolution or interactions in the case of N-coupled stochastic nonlinear Schrödinger equations. In particular, we will focus on the case of $N=3$ and $N=4$, respectively.

4.4.1 System of three coupled stochastic NLS equations

Consider the following system of three coupled stochastic NLS equations (see [5] for the deterministic system):

https://doi.org/10.4208/cicp.300815.180416a Published online by Cambridge University Press

$$\begin{aligned}
&\mathrm{i}\mathrm{d}u_t+ku_{xx}\mathrm{d}t+(\sigma|u|^2+\beta|v|^2+\sigma|w|^2)u\mathrm{d}t=\varepsilon u\circ\mathrm{d}W(t),\\
&\mathrm{i}\mathrm{d}v_t+kv_{xx}\mathrm{d}t+(\beta|u|^2+\sigma|v|^2+\beta|w|^2)v\mathrm{d}t=\varepsilon v\circ\mathrm{d}W(t),\\
&\mathrm{i}\mathrm{d}w_t+kw_{xx}\mathrm{d}t+(\sigma|u|^2+\beta|v|^2+\sigma|w|^2)w\mathrm{d}t=\varepsilon w\circ\mathrm{d}W(t),
\end{aligned}\tag{4.4}$$

together with initial data:

$$\begin{aligned}
u(x,0)&=a_0[1-\xi\cos(lx)],\\
v(x,0)&=b_0[1-\xi\cos(l(x+\theta))],\\
w(x,0)&=c_0[1-\xi\cos(lx)],
\end{aligned}$$

where $k=1$, $\sigma=1$, $\beta=1$, $a_0=0.3$, $b_0=0.3$, $c_0=0.3$, $\xi=0.1$, $l=0.5$, $\theta=0$.

In this experiment, the space-time domain $[0,8\pi]\times[0,100]$ is divided with $h=\pi/100$ and $\tau=0.01$. The surface and contour plots of the wave solutions via the compact scheme (3.1) with various sizes of noise are shown in Fig. 13. Note that in the case of three coupled equations we choose the value of ε smaller than that of two coupled case, since for $\varepsilon=0.03$ the shape of soliton is hardly to be recognized; see the bottom figures in Fig. 13. In the deterministic case ($\varepsilon=0$), we can see that the soliton waves show periodic behavior. However, we observe that in the case $\varepsilon=0.005$, the peaks of $|u|+|v|+|w|$ have shifted and the periodic behavior of soliton waves has disappeared even though the shape of soliton is easy to recognize. Moreover, it presents more peaks in the considered domain than the deterministic case. For $\varepsilon=0.01$, the shape of solitons could still be identified, but there are more oscillations in the solitons and more peaks than the deterministic case. At $\varepsilon=0.03$, it is hard for us to recognize the shape of solitons and it is almost destroyed. It seems that the solitons of three coupled equations are more sensitive to the perturbation of noise than that of the two coupled case.

4.4.2 System of four coupled stochastic NLS equations

To investigate the interaction scenarios of four solitons with different wave amplitudes, different velocities and different sizes of noise, we consider the following coupled system

$$\begin{aligned}
&\mathrm{i}\mathrm{d}u_t+ku_{xx}\mathrm{d}t+[\sigma|u|^2+\beta(|v|^2+|p|^2+|q|^2)]u\mathrm{d}t=\varepsilon u\circ\mathrm{d}W(t),\\
&\mathrm{i}\mathrm{d}v_t+kv_{xx}\mathrm{d}t+[\sigma|v|^2+\beta(|u|^2+|p|^2+|q|^2)]v\mathrm{d}t=\varepsilon v\circ\mathrm{d}W(t),\\
&\mathrm{i}\mathrm{d}p_t+kp_{xx}\mathrm{d}t+[\sigma|p|^2+\beta(|u|^2+|v|^2+|q|^2)]p\mathrm{d}t=\varepsilon p\circ\mathrm{d}W(t),\\
&\mathrm{i}\mathrm{d}q_t+kq_{xx}\mathrm{d}t+[\sigma|q|^2+\beta(|u|^2+|v|^2+|p|^2)]q\mathrm{d}t=\varepsilon q\circ\mathrm{d}W(t),
\end{aligned}\tag{4.5}$$

together with the initial conditions:

$$\begin{aligned}
u(x,0)&=\sqrt{2}r_1\mathrm{sech}(r_1x+x_{10})e^{\mathrm{i}v_1x},\\
v(x,0)&=\sqrt{2}r_2\mathrm{sech}(r_2x-x_{10})e^{-\mathrm{i}v_2x},\\
p(x,0)&=\sqrt{2}r_3\mathrm{sech}(r_3x+x_{30})e^{\mathrm{i}v_3x},\\
q(x,0)&=\sqrt{2}r_4\mathrm{sech}(r_4x-x_{30})e^{-\mathrm{i}v_4x}.
\end{aligned}$$

https://doi.org/10.4208/cicp.300815.180416a Published online by Cambridge University Press

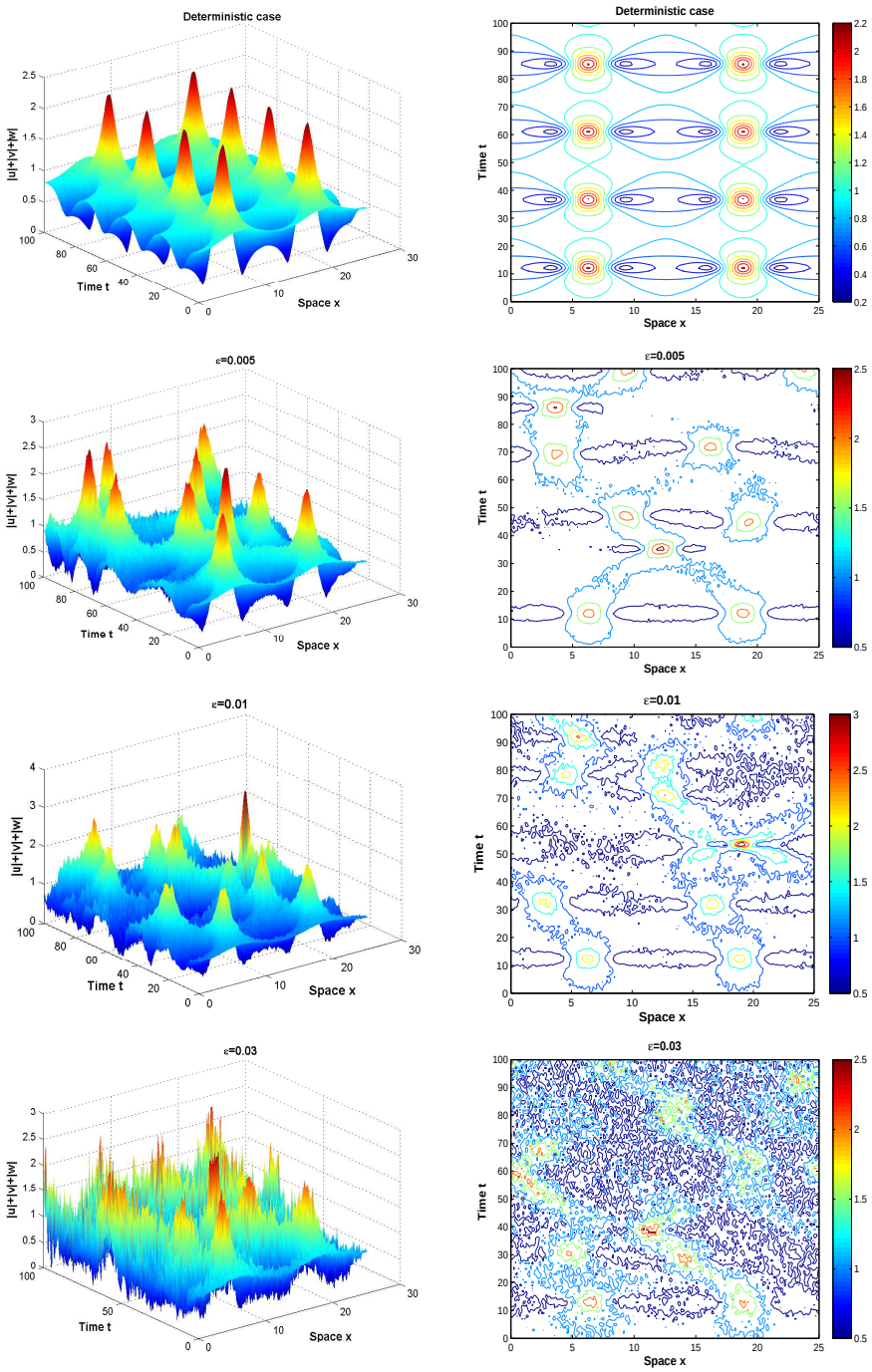


Figure 13: The surface and contour plots of interaction scenario of $|u|+|v|+|w|$ with $\varepsilon=0.005,\ 0.01,\ 0.03$, respectively.

https://doi.org/10.4208/cicp.300815.180416a Published online by Cambridge University Press

In the following numerical computations we choose $k=1$, $\sigma=1$, $r_1=r_2=1$, $r_3=r_4=1.4$, $v_1=v_2=\eta/8$, $v_3=v_4=\eta/4$, $T=100$, $a=-50$, $b=50$, $h=1/12$, $\tau=0.01$ and the initial position parameters $x_{10}=10$ and $x_{30}=40$.

In the first test we select the control parameters $\beta=1$ and $\eta=1$ such that the four profiles in the initial data will keep their own propagation after interaction with each other in the deterministic case. We present the interaction scenario of four solitons with different amplitudes of noise $\varepsilon=0.01,\ 0.03,\ 0.05$ in Fig. 14 with the help of surfaces and contour plots. It can be observed that the four solitons march with their own velocities and shapes before their collision. They will not meet at the same time. However, from the contours we see that the velocities, amplitudes and shapes of the solitons have changed due to the existence of noise. In addition, we can observe that the propagation directions of the four solitons have changed which are effected by the noise. This phenomenon will have an influence on the interaction of solitons, e.g., the position and time where and when solitons collide with each other. The amplitudes of the pulses at different time t are depicted in Figs. 15-17. From these figures, we recover the observation that the small noise does not introduce too much influence on the soliton in the short time interval while for longer time or for stronger noise, the inelastic interaction between solitons and waves generated by the noise leads to strong perturbation, and could even destroy solitons.

For the second test we choose the parameters β=0.25, η=0.8 such that the four profiles in the initial data will fuse into a single soliton after their collision in the deterministic case. We present the fusion scenario of four solitons at different sizes ε of noise in Fig. 18. From this figure, we see that the noise does not change the intrinsic fusion character of solitons, but the noise has an influence on the direction of each soliton, which affects the fusion order of solitons.

We select the parameters $\beta=2$, $\eta=1.6$ in the third set of computations so that new waves will be created after their collision of four profiles in the initial data in the deterministic case (Fig. 19), which is the result of the large value of β and moderate collision velocity. We present the creation scenario of four solitons, respectively, with different sizes of noise $\varepsilon=0.01,\ 0.03$ and 0.05 in Figs. 20-22. From Fig. 20, we observe that the effect on components p and q is stronger than that on u, v for small noise $\varepsilon=0.01$. As the increase of amplitude of noise, the influence of noise on the soliton gets significant.

4.5 Mean-square convergence order

We investigate the convergence order in temporal direction of the proposed compact scheme for two coupled stochastic NLS equations in this experiment. Define

$$e^u_{\Delta t}:=\left(\mathbb{E}\|u(\cdot,T)-u_T(\cdot)\|^2_{\mathbb{L}^2}\right)^{\frac{1}{2}},\quad e^v_{\Delta t}:=\left(\mathbb{E}\|v(\cdot,T)-v_T(\cdot)\|^2_{\mathbb{L}^2}\right)^{\frac{1}{2}},$$

let $\sigma=1$, $\alpha=1$, $[x_L,x_R]=[-1,1]$, $\Delta x=\frac{1}{200}$, $T=\frac{1}{4}$ and $u|_{t=0}=\sin(\pi x)$, $v|_{t=0}=\sin(\pi x)$, and plot $e^u_{\Delta t}$, $e^v_{\Delta t}$ against Δt on a log-log scale with various combinations of $(\beta,\ \varepsilon)$ for the truncated number of Wiener process $1\le M\le 8$ of Eq. (2.1), respectively. Although we

https://doi.org/10.4208/cicp.300815.180416a Published online by Cambridge University Press

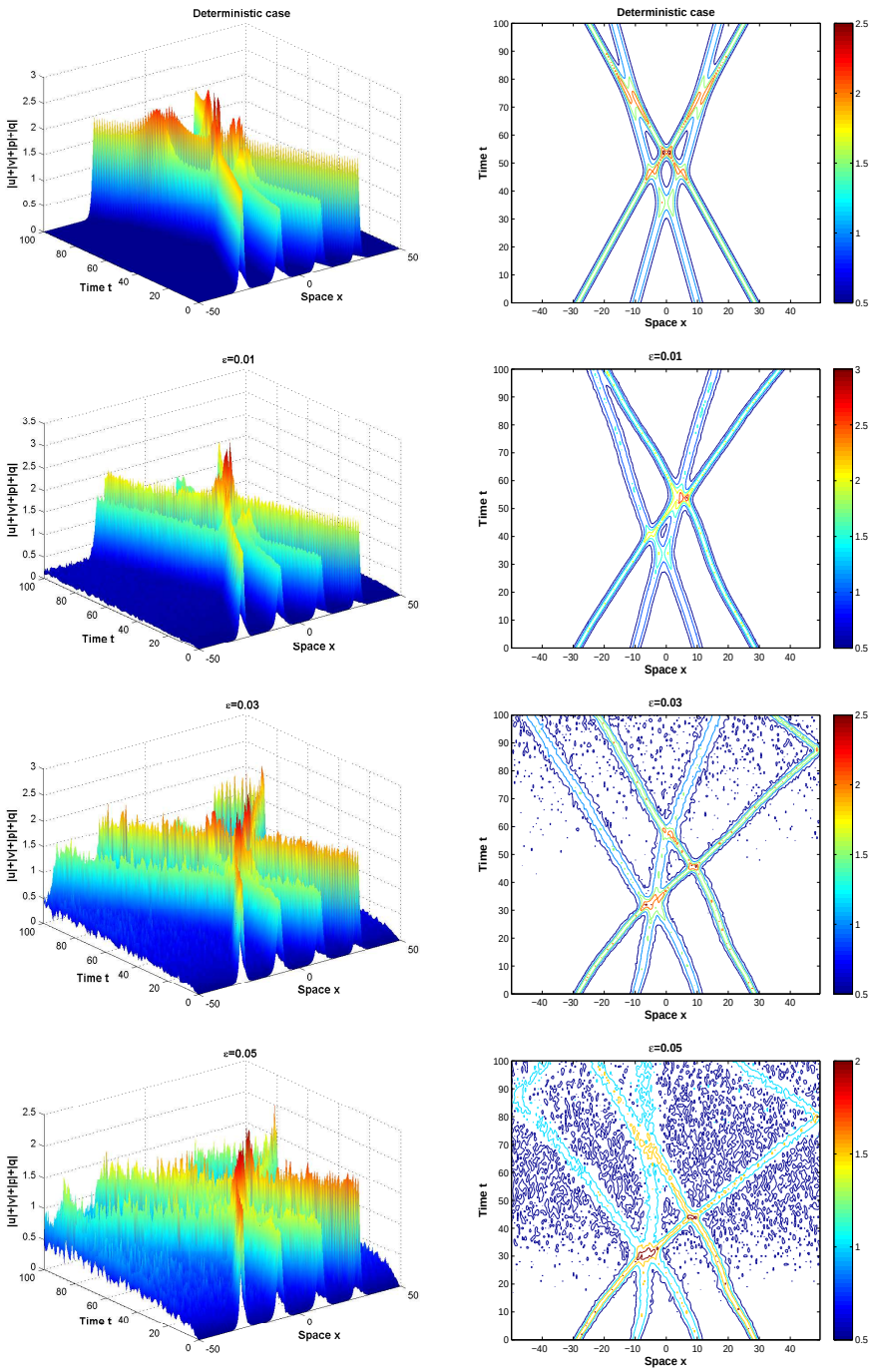


Figure 14: The surface and contour plots of interaction scenario of $|u|+|v|+|p|+|q|$ with $\varepsilon=0.01,\ 0.03,\ 0.05$, respectively.

https://doi.org/10.4208/cicp.300815.180416a Published online by Cambridge University Press

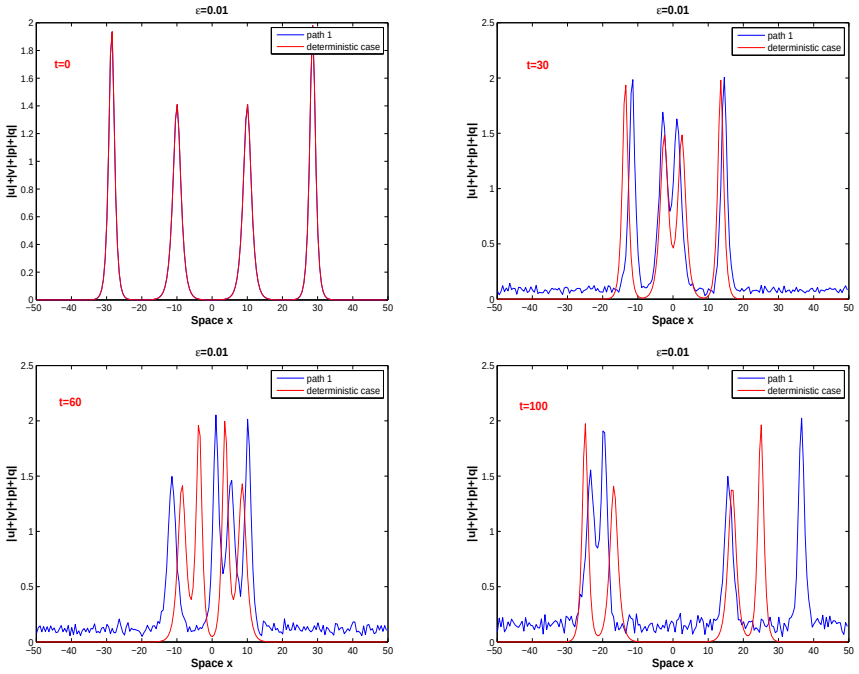


Figure 15: Collision of four solitons along one trajectory with $\varepsilon = 0.01$.

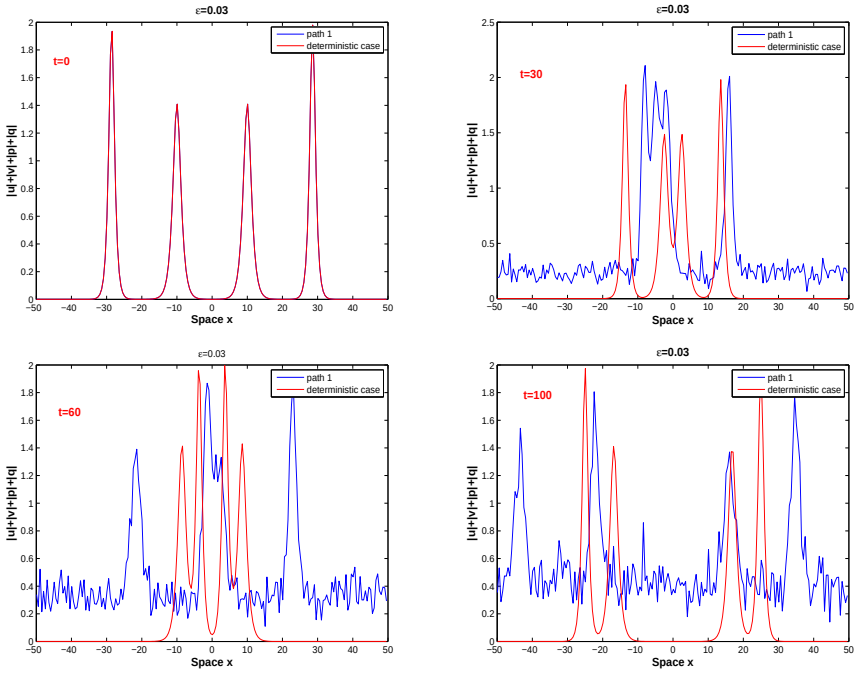


Figure 16: Collision of four solitons along one trajectory with $\varepsilon = 0.03$.

https://doi.org/10.4208/cicp.300815.180416a Published online by Cambridge University Press

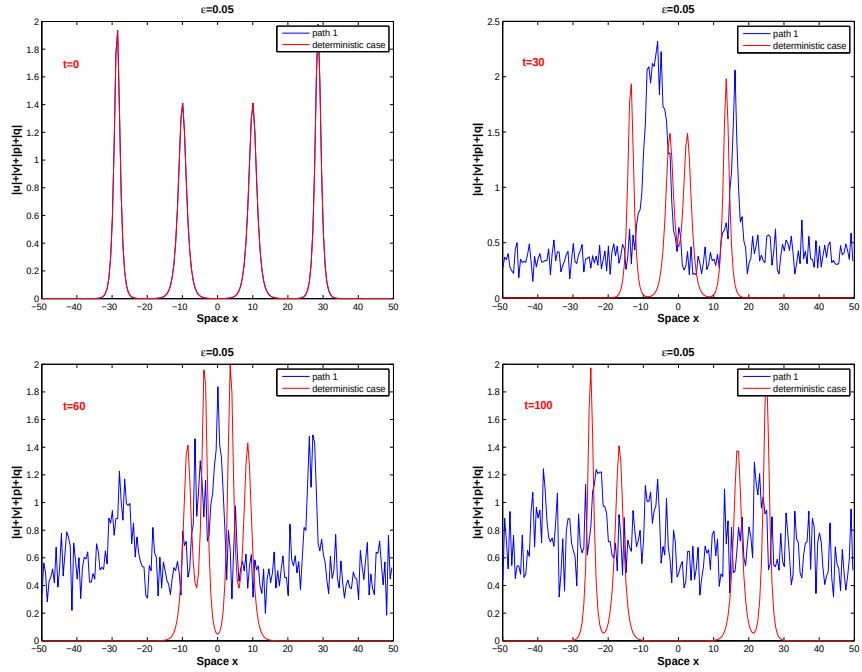


Figure 17: Collision of four solitons along one trajectory with $\varepsilon=0.05$.

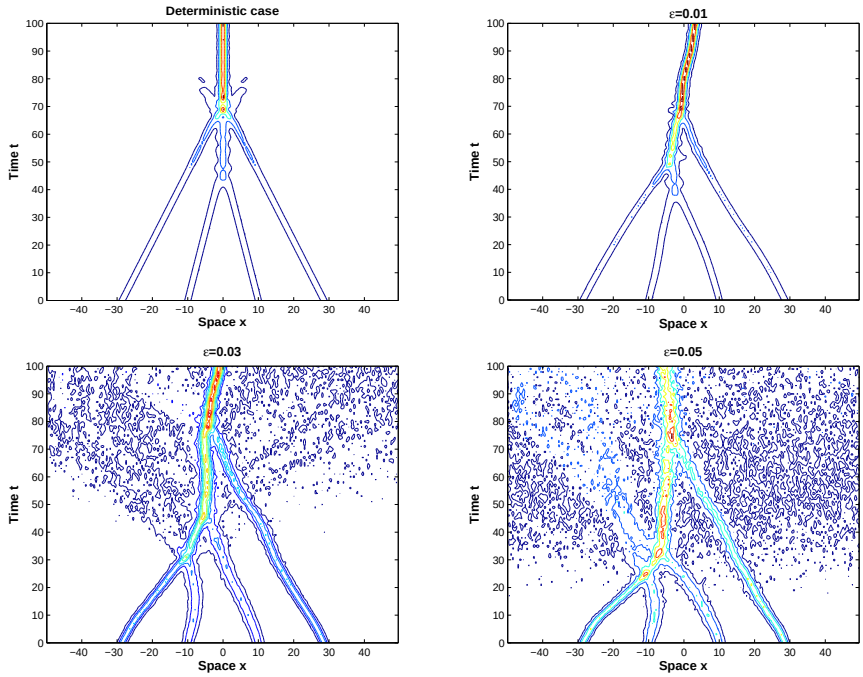


Figure 18: Fusion scenario of $|u|+|v|+|p|+|q|$ with $\varepsilon=0.01,\ 0.03,\ 0.05$.

https://doi.org/10.4208/cicp.300815.180416a Published online by Cambridge University Press

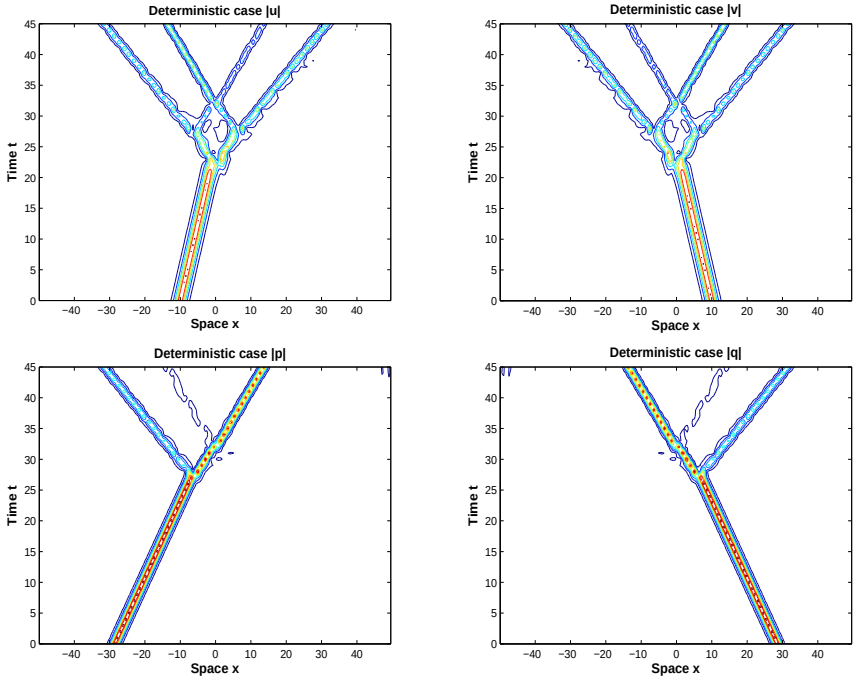


Figure 19: Creation scenario of $|u|$, $|v|$, $|p|$ and $|q|$ in the deterministic case.

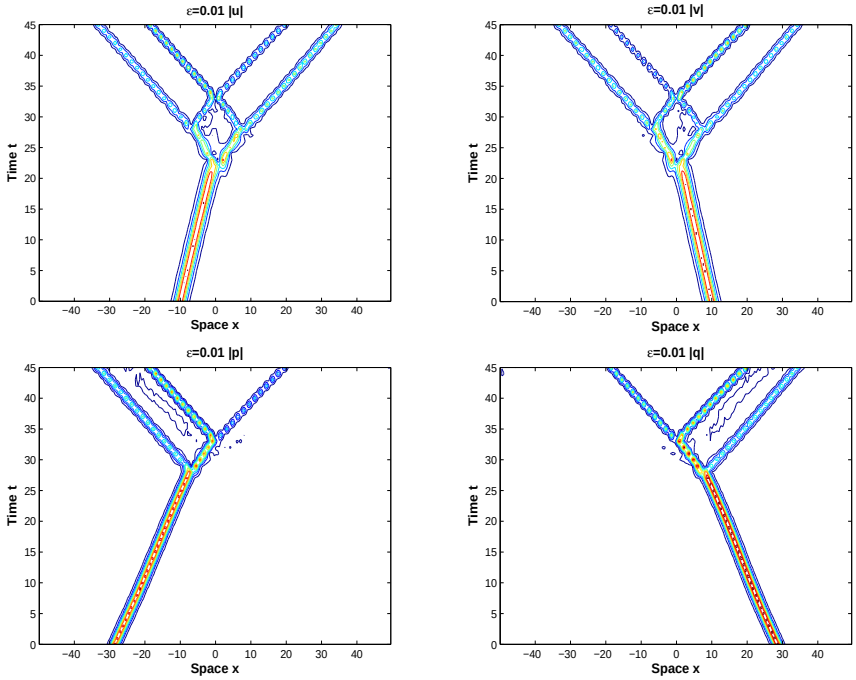


Figure 20: Creation scenario of $|u|$, $|v|$, $|p|$ and $|q|$ with $\varepsilon=0.01$.

https://doi.org/10.4208/cicp.300815.180416a Published online by Cambridge University Press

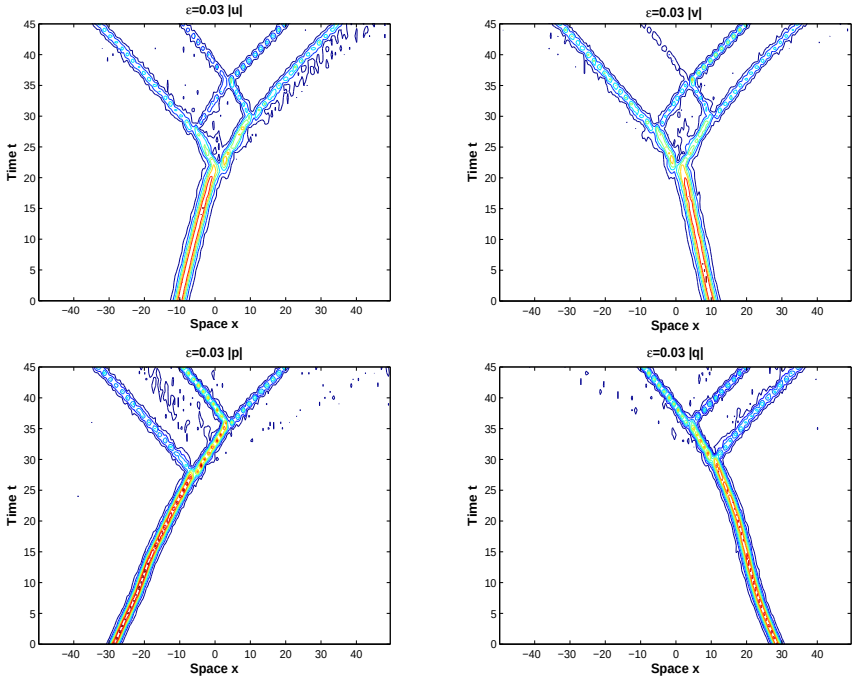


Figure 21: Creation scenario of $|u|$, $|v|$, $|p|$ and $|q|$ with $\varepsilon=0.03$.

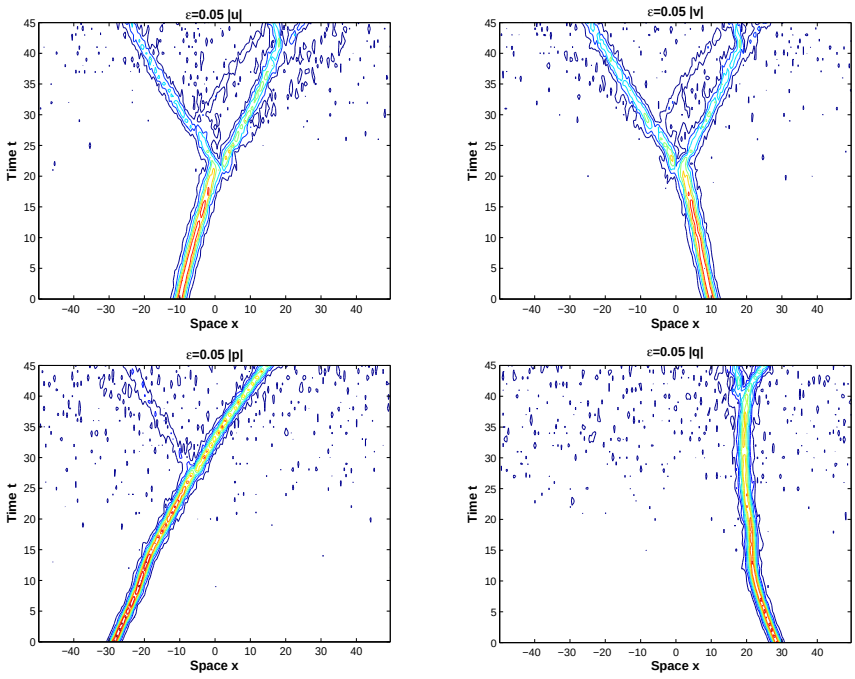


Figure 22: Creation scenario of $|u|$, $|v|$, $|p|$ and $|q|$ with $\varepsilon=0.05$.

https://doi.org/10.4208/cicp.300815.180416a Published online by Cambridge University Press

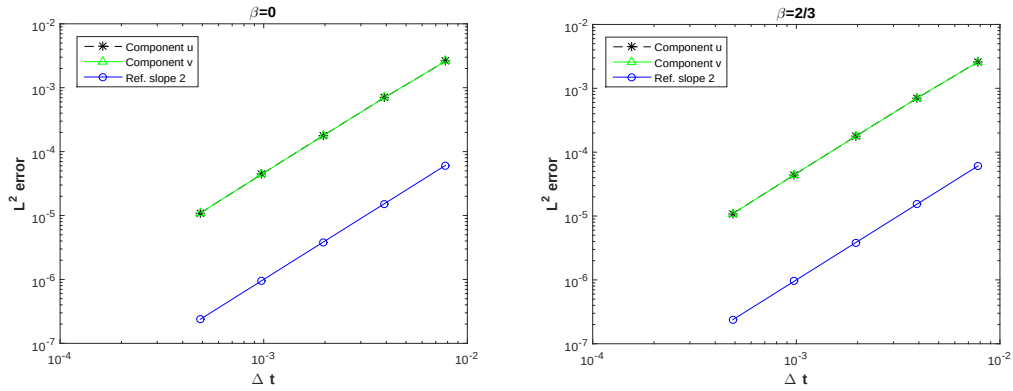


Figure 23: Rates of convergence for the deterministic case with $\beta=0$ and $\beta=2/3$, respectively.

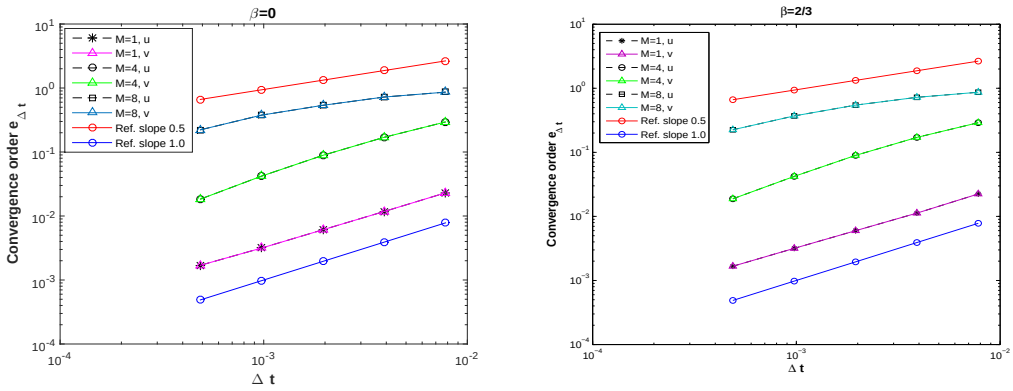


Figure 24: Mean square error versus time steps with $\beta=0$ and $\beta=2/3$ for $1\leq M\leq 8$, respectively.

do not know the explicit form of the solution to (1.2), we take the compact scheme with the very small time stepsize $\Delta t=2^{-14}$ as a reference solution. We then compare it to the compact scheme evaluated with time steps $(2^1\Delta t,2^3\Delta t,2^5\Delta t,2^7\Delta t)$ in order to estimate the rate of convergence.

We consider $\varepsilon=0$ first: Fig. 23 shows order 2 for the $\mathbb{L}^2$-error of the compact for different sizes of β.

The observations are different in the stochastic case ($\varepsilon=\sqrt{2}$) where different sorts of Wiener processes depending on M are used. Fig. 24 presents the mean-square convergence order for the $\mathbb{L}^2$-error with various sizes of β. And 200 realizations are chosen to approximate the expectations. As is displayed in Fig. 24, the strong order of convergence drops from approximately 1 to 0.5 for values 1 to 8 of M. It is an interesting and open problem to investigate theoretically the convergence order of the proposed compact scheme.

https://doi.org/10.4208/cicp.300815.180416a Published online by Cambridge University Press

5 Conclusions

In this paper, we propose a compact scheme to the coupled stochastic nonlinear Schrödinger equations. We prove that the compact scheme preserves the discrete stochastic multi-symplectic conservation law, discrete charge conservation law and discrete energy evolution law almost surely. Numerical experiments confirm well the theoretical analysis results. Moreover, we have performed a detailed numerical investigation of the effect of a random potential on the evolutions and interactions of solitons in this paper. Especially, we have studied the evolution of a single soliton, collision of multi-solitons and the splitting of a profile into more solitons with different amplitudes of noise. Of physical and optical interest, relevant properties of soliton interactions in the systems of 3-CSNLS and 4-CSNLS have been analyzed and graphically discussed.

The compact scheme which is proposed in this paper has lots of merits. However, in the stochastic situation, the solution is not expected to be smooth either in space or in time. Therefore, studying the convergence of the compact scheme for CSNLS equations is of great mathematical interest. We have studied the convergence order in temporal direction of the proposed compact scheme numerically. And it is an interesting open problem to study theoretically the convergence order of the compact scheme.

Acknowledgments

This work was supported by the National Natural Science Foundation of China (Nos. 91530118, 91130003, 11021101, 11290142, 11471310, 11601032, 11301234, 11271171), the Provincial Natural Science Foundation of Jiangxi (Nos. 20142BCB23009, 20161ACB20006, 20151BAB201012).

References

[1] P.G. Drazin, *Solitons, in: London Mathematical Society Lecture Note Series*, Cambridge University Press, Cambridge, 1983.
[2] A. Debussche and L.D. Menza, *Numerical simulation of focusing stochastic nonlinear Schrödinger equations*, Physica D, **162** (2002), 131-154.
[3] J.N. Elgin, *Stochastic perturbations of optical solitons*, Opt. Lett., **18** (1993), 10-12.
[4] J.P. Gordon, *Interacion forces among solitons in optical fibers*, Opt. Lett., **8** (1983), 596-598.
[5] A. Hasegawa, *Optical solitons in fibers*, Springer Berlin Heidelberg, 1989.
[6] E. Hairer, C. Lubich and G. Wanner. *Geometric numerical integration*, New York: Springer-Verlag, 2006.
[7] S. Jiang, L. Wang and J. Hong, *Stochastic multi-symplectic integrator for stochastic nonlinear Schrödinger equation*, Commun. Comput. Phys., **14** (2013), 393-411.
[8] Y. Kodama, M. Romagnoli and S. Wabnitz, *Soliton stability and interactions in fibre lasers*, Electron. Lett., **28** (1992), 1981-1983.
[9] L. Kong, J. Hong, L. Ji and P. Zhu, *Compact and efficient conservative schemes for coupled nonlinear Schrödinger equations*, Numer. Methods Partial Differential Eq., **31** (2015), 1814-1843.

https://doi.org/10.4208/cicp.300815.180416a Published online by Cambridge University Press

[10] W. Liu, N. Pan, L. Huang and M. Lei, *Soliton interactions for coupled nonlinear Schrödinger equations with symbolic computation*, Nonlinear Dynam., **78** (2014), 755-770.
[11] S.K. Lele, *Compact finite difference schemes with spectral-like resolution*, J. Comput. Phys., **103** (1992), 16-42.
[12] F.M. Mitschke and L.F. Mollenauer, *Experimental observation of interaction forces between solitons in optical fibers*, Opt. Lett., **12** (1987), 355-357.
[13] B.A. Malomed, *Bound solitons in coupled nonlinear Schrödinger equations*, Phys. Rev. A, **45** (1992), R8321.
[14] J. Sun, X. Gu and Z. Ma, *Numerical study of the soliton waves of the coupled nonlinear Schrödinger system*, Physica D, **196** (2004), 311-328.
[15] Z. Sun, Y. Gao, X. Yu and Y. Liu, *Switching of bound vector solitons for the coupled nonlinear Schrödinger equations with nonhomogenously stochastic perturbations*, Chaos, **22** (2012), 043132.
[16] T. Ueda and W.L. Kath, *Dynamics of optical pulses in randomly birefringent fibers*, Physica D, **55** (1992), 166-181.
[17] P.K.A. Wai, C.R. Menyuk and H. Chen, *Stability of solitons in randomly varying birefringent fibers*, Opt. Lett., **16** (1991), 1231-1233.

https://doi.org/10.4208/cicp.300815.180416a Published online by Cambridge University Press